

Magnetic dipolar ordering and relaxation in the high-spin molecular cluster compound Mn_6

A. Morello,* F. L. Mettes, O. N. Bakharev, H. B. Brom, and L. J. de Jongh

Kamerlingh Onnes Laboratory, Leiden Institute of Physics, Leiden University, P.O. Box 9504, 2300 RA Leiden, The Netherlands

F. Luis and J. F. Fernández

Instituto de Ciencia de Materiales de Aragón, CSIC-Universidad de Zaragoza, 50009 Zaragoza, Spain

G. Aromí

Departament de Química Inorgànica, Universitat de Barcelona, Av. Diagonal 647, 08028 Barcelona, Spain

(Received 8 September 2005; revised manuscript received 21 February 2006; published 5 April 2006)

Few examples of magnetic systems displaying a transition to pure dipolar magnetic order are known to date. As was recently shown, within the newly discovered class of single-molecule magnets, quite attractive examples of dipolar magnetism may be found. The molecular cluster spins and thus their dipolar interaction energy can be quite high, leading to reasonably accessible ordering temperatures even for sizable intercluster distances. In favorable cases bonding between clusters in the molecular crystal is by van der Waals forces only, and no exchange paths of importance can be distinguished. An important restriction, however, is the requirement of sufficiently low crystal field anisotropy for the cluster spin, in order to prevent the occurrence of superparamagnetic blocking at temperatures above the dipolar ordering transition. This condition can be met for molecular clusters of sufficiently high symmetry, as for the Mn_6 molecular cluster compound studied here. The uniaxial anisotropy of the cluster spin $S=12$ is as small as $D/k_B=0.013$ K, giving a total zero-field splitting of the $S=12$ multiplet of 1.9 K. As a result, the electron-spin lattice relaxation time remains fast ($\sim 10^{-4}$ s) down to T_c and no blocking occurs. Magnetic specific heat and susceptibility experiments show a transition to ferromagnetic dipolar order at $T_c=0.16$ K. Classical Monte Carlo calculations, performed for Ising $S=12$ dipoles on a lattice do predict ferromagnetic ordering and account for the value of T_c as well as the shape of the observed specific heat anomaly. By applying magnetic fields up to 6 T the hyperfine contributions C_{hf} to the specific heat arising from the ^{55}Mn nuclei could be detected. From the time dependence of the measured C_{hf} the nuclear-spin lattice relaxation time T_{1n} could be determined for the same field range in the temperature region $0.2 < T < 0.6$ K. The nuclear magnetic relaxation was further studied by high field ^{55}Mn pulse NMR measurements of both the nuclear T_{1n} and T_{2n} at $T=0.9$ K (up to 7 T). The data are in good mutual agreement and can be well described by the theory for magnetic relaxation in highly polarized paramagnetic crystals and for dynamic nuclear polarization, which we extensively review. The experiments provide an interesting comparison with the recently investigated nuclear spin dynamics in the anisotropic single-molecule magnet Mn_{12} -ac.

DOI: [10.1103/PhysRevB.73.134406](https://doi.org/10.1103/PhysRevB.73.134406)

PACS number(s): 75.10.Jm, 75.30.Kz, 76.60.-k

I. INTRODUCTION

Experimental and theoretical interest in magnetic molecular clusters carrying a net high spin has rapidly evolved in recent years (for reviews see, e.g., Refs. 1–5). Since the cores of these molecules can be viewed as nanosized pieces of magnetic insulators, they offer attractive possibilities to study magnetic objects of dimensions in between atom and bulk. Of great importance is the fact that these (macro)molecules form stoichiometric chemical compounds, which may crystallize as molecular crystals, implying that for a given compound identical magnetic molecules are arranged on the sites of a regular three-dimensional (3D) lattice. More often than not, there is only a single molecular site per unit cell, so that the symmetry axes of all molecules in the crystal are perfectly aligned. Provided that the intermolecular magnetic interactions are sufficiently weak, macroscopic solid state techniques can then be exploited to study the properties of individual cluster spins, taking into account their couplings to the “environment” (phonons, nuclear moments) as perturbations. Accordingly, such experiments have already pro-

vided highly interesting information about the quantum tunneling properties of the cluster spins.^{6–16}

On the other hand, the long-range magnetic ordering (LRMO) phenomena expected to occur at sufficiently low temperatures as a consequence of the intercluster magnetic dipolar coupling present an interesting object of study in itself.^{17,18} In many of these compounds, the clusters are only or mainly coupled by van der Waals forces in the molecular crystal. Short-ranged superexchange interactions may then be neglected, leaving only the dipolar coupling between cluster spins as a source for producing LRMO. Since in the literature of magnetic phase transitions few examples of LRMO produced purely by dipolar forces are yet available,^{19–21} the chance to exploit molecular magnets to this end is quite attractive and could represent an important contribution to this field.

However, for most high-spin molecules studied so far, such as Mn_{12} ,²² Fe_8 ,²³ and the Mn_4 family of compounds,^{24–26} the cluster spins have strong Ising-type anisotropy, associated with the zero-field splitting (ZFS) of the magnetic energy levels by the action of the crystal field. As a

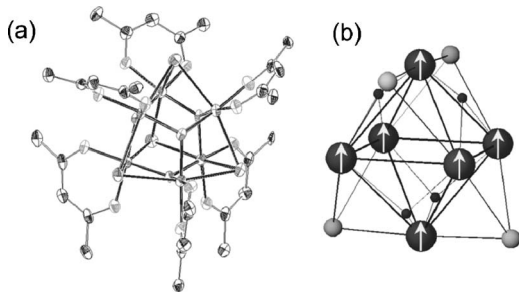


FIG. 1. (a) Structure of $\text{Mn}_6\text{O}_4\text{Br}_4(\text{Et}_2\text{dbm})_6$; (b) sketch of the symmetric octahedral core, containing six ferromagnetically coupled Mn^{3+} ions, yielding a total spin $S=12$ for this molecular superparamagnetic particle. The gray and black spheres indicate the Br^- and O^{2-} ions respectively. The white arrows illustrate the ferromagnetic alignment of the Mn^{3+} $s=2$ spins inside the cluster.

consequence, the cluster spins become frozen below a blocking temperature, T_B , of typically a few K, with the spin direction randomly distributed between the two possible orientations along the easy axis. Evidently, this superparamagnetic blocking process is in competition with intercluster magnetic interactions that tend to establish LRMO at (usually much) lower temperatures. Although it has been shown theoretically²⁷ that the occurrence of quantum tunneling between opposite spin directions at temperatures below T_B may in principle produce sufficient fluctuations to overcome blocking, in most of the investigated anisotropic molecules the times involved for the actual observation of the ensuing LRMO are still much too long. The recently discovered example of LRMO found at $T_c=0.21$ K in the molecular magnet Mn_4Me is an exception rather than the rule.²⁸

The obvious route to find dipolar-induced LRMO in molecular magnetic cluster compounds is, therefore, to search for high-spin molecules with as low anisotropy as possible and with negligible superexchange interactions. In a preliminary report²⁹ on the compound $\text{Mn}_6\text{O}_4\text{Br}_4(\text{Et}_2\text{dbm})_6$ (hereafter called Mn_6) we could show that it provides an excellent example. The Mn_6 molecule has a highly symmetric cluster core, comprising an octahedron of Mn^{3+} ions the faces of which are capped by O^{2-} or Br^- ions. The structure of the molecule³⁰ and a sketch of its octahedral core are shown in Fig. 1. From previous magnetic studies³⁰ above 2 K it was found that the superexchange paths formed between the Mn^{3+} ions (each having atomic spin $s=2$) through the intervening O^{2-} and Br^- ligands result in a relatively strong ferromagnetic interaction, of value $J_f/k_B \sim +13$ K on basis of the pair Hamiltonian $\mathcal{H}=-2J\mathbf{S}_i \cdot \mathbf{S}_j$. As a consequence, the ground state is a $S=12$ multiplet and the energy of the nearest excited state is approximately 150 K higher. The unit cell is monoclinic, with space group Pc , and contains four molecules that have such a high (nearly T_d) symmetry that the net anisotropy for the cluster spin is quite small. No superexchange paths connecting neighboring clusters can be discerned indeed in the crystal structure, so that we can safely assume that the crystal binding arises solely from van der Waals bonds. We note that, although intercluster magnetic ordering has also been reported for the molecular magnets Fe_{19} ³¹ and Mn_4Br ,³² in those cases superexchange between

clusters apparently plays an important role, as evidenced, e.g., by the much higher T_c values found (1.2–1.3 K). However, for a Cr_4S cluster,³³ for which the intracluster exchange between the Cr^{3+} ions happens to be likewise ferromagnetic (net spin $S=6$), the low value of $T_c=0.17$ K that was observed could be compatible with dipolar-induced magnetic ordering, in this case of antiferromagnetic type. More data would be needed, however, to substantiate this.

In a preliminary report,²⁹ we could already show that the magnetic anisotropy in Mn_6 is sufficiently low to enable measurements of its magnetic susceptibility and specific heat under thermal equilibrium conditions down to the lowest temperatures reached ($T \approx 15$ mK) by our experimental setups. The data did evidence a transition to LRMO, as hoped for, at a temperature of $T_c=0.16$ K, corresponding apparently to a ferromagnetic arrangement of the cluster moments. Comparison with Monte Carlo simulations strongly supported the expected dipolar origin of the intercluster coupling. When applying magnetic fields of up to 6 T, the study of the time-dependent magnetic specific heat revealed a transition from fast relaxation to nonequilibrium conditions within the experimental time window of 1–100 s.

In the present work we extend these experimental and theoretical studies and discuss in much more detail the results and conclusions. In addition, we have performed ^{55}Mn NMR studies in varying field, enabling to draw more definite conclusions about the magnetic relaxation of both electronic and nuclear spin systems in this material. The nuclear spin-lattice relaxation time is governed by fluctuations of the cluster electronic spins, and is indeed quite fast in zero field. By applying a magnetic field these fluctuations become progressively suppressed as a consequence of the Zeeman splitting of the electronic energy levels, thereby bringing the nuclear spin system out of thermal equilibrium. This provides an interesting comparison with recent zero-field ^{55}Mn NMR studies^{34–37} of the anisotropic molecular magnet $\text{Mn}_{12}\text{-ac}$, for which the suppression of the magnetic relaxation in the thermally activated regime can be fully ascribed to the strong splitting of the cluster spin levels by the crystal field. For the present compound, crystal-field splittings play a very minor role in the relaxation process, except for providing the necessary channel for energy transfer between spins and lattice phonons. We present a full analysis of the longitudinal and transverse nuclear relaxation in terms of previously developed theories for relaxation by paramagnetic impurities and for dynamic polarization, taking into account electron spin fluctuations by both spin-lattice relaxation and spin-spin interactions. Our NMR data in high fields prove to be in excellent qualitative as well as quantitative agreement with such theoretical predictions. The values for the longitudinal nuclear spin-lattice relaxation rate and for the effective hyperfine interaction constant deduced from our high-field time-dependent specific heat data are likewise in good accord with the NMR results.

The outline of this paper is as follows. After giving a few experimental details in the next section, the measured susceptibility and zero-field specific heat data are presented and discussed in Secs. III A and III B, followed by a Monte Carlo simulation study of the zero-field specific heat in Sec. III C. In Sec. III D the field-dependent specific heat measure-

ments are discussed, followed by the nuclear resonance and nuclear relaxation data in Sec. III E. Section IV contains an analysis of these data in terms of existing theoretical models for relaxation in highly polarized magnetic systems. Concluding remarks are given in Sec. V, while in the Appendix we describe the calculation of the demagnetizing factor for powder samples. Systeme International units will be used throughout the paper.

II. EXPERIMENTAL DETAILS

Polycrystalline samples of Mn_6 were prepared as reported in Ref. 30. Low-temperature specific heat measurements were performed in a homemade calorimeter that makes use of the thermal relaxation method.^{5,15,38} For the measurements, a few milligrams of sample were mixed with Apiezon N grease and placed on the sapphire plate of the calorimeter. Details of this measurement technique are given in Ref. 38. An important advantage of this method is that the characteristic time τ_e of the experiment (typically, $\tau_e \approx 0.1$ –1000 seconds at low T) can be varied (within limits) by changing the dimensions (and therefore the thermal resistance) of the Au wire that acts as a thermal link between the calorimeter and the mixing chamber of the dilution refrigerator. Magnetic fields up to 16 T can be applied with a superconducting magnet and the lowest temperatures reached are of the order of 50 mK.

The ac-susceptibility measurements were performed between 15 mK and 4 K in a homemade susceptometer, placed inside the plastic mixing chamber of a dilution refrigerator and thermalized by the ^3He flow.³⁷ The susceptometer, based on the mutual inductance technique, consists of a primary coil with 250 turns of $\varnothing 100 \mu\text{m}$ NbTi wire, and two oppositely wound secondary coils, each with 660 turns of $\varnothing 40 \mu\text{m}$ Cu wire. By placing the sample inside one of the two secondary coils and feeding the primary with an ac current (typically $\sim 50 \mu\text{A}$), the induced voltage across the secondary is proportional to the susceptibility of the sample. By phase-sensitive detection we can also discriminate the real and imaginary parts of the susceptibility. The excitation frequency ν was varied between 230 and 7700 Hz. Additional measurements above 1.8 K were performed using the ac option of a commercial superconducting quantum interference device (SQUID) magnetometer.

As for the NMR experiments, we introduced the sample and the four-turns NMR coil inside the plastic ^3He pot of a pumped ^3He cryostat, where variable magnetic fields up to 8 T could be applied by a superconducting magnet. The resonance of the ^{55}Mn nuclei of Mn_6 was observed by means of the spin-echo technique, with a typical duration of the $\pi/2$ pulse of $t_{\pi/2} \sim 2 \mu\text{s}$.

Estimates of the magnitude of the magnetic anisotropy have been obtained as follows. Magnetic data measured above 1.8 K (Ref. 30) can be fitted by expressions valid for fully isotropic $S=12$ spins, i.e., they do not evidence any detectable ZFS for the total spin. The data are excellently fitted by the Brillouin curve calculated for an isotropic paramagnet with $S=12$ and $g=1.98$ [as derived from electron paramagnetic resonance (EPR)]. If we write a single-spin Hamiltonian for the molecule as

$$\mathcal{H} = -DS_z^2 - g\mu_B \mathbf{B}_a \cdot \mathbf{S}, \quad (1)$$

these experiments provide an upper limit of $|D|/k_B \leq 0.01$ K.³⁰ In order to obtain an independent estimation of D , high-frequency EPR experiments were carried out at the NHMFL in Tallahassee by Krzystek, using several frequencies in the range 95–380 GHz. Simulations of the spectra performed using Eq. (1) agree well with the experimental results for $0.01 \text{ K} < |D|/k_B < 0.05 \text{ K}$. A value of $|D|/k_B \approx 0.01 \text{ K}$ seems therefore appropriate to describe the ZFS in Mn_6 . When discussing the ac susceptibility and specific heat data in Secs. III A and III B we shall adopt the value $D/k_B = 0.013 \text{ K}$, which yields the best agreement between theory and experiment for both techniques.

The isotropic character of the molecular spin might seem paradoxical at first, considering that the individual Mn^{3+} ions, being Jahn-Teller ions, experience strong anisotropy: typical values of $|D|/k_B$ for the ion are a few tenths of Kelvin. However, the net D value entering in the spin Hamiltonian for the cluster can be seen in first approximation to result from the vectorial addition of the local anisotropy tensors of the individual ions, which then can give rise to a low net anisotropy for highly symmetric molecules such as Mn_6 (cf. Fig. 1), even for large ZFS of the constituting atoms.³⁹ In fact, the possibility to tune the net anisotropy of the cluster spin by means of molecular synthesis is one of the attractive properties of these nanosized molecular superparamagnets.

III. EXPERIMENTAL RESULTS AND ANALYSES

A. Magnetic susceptibility

Strong evidence for the long-range ordering of the magnetic moments is provided by the magnetic susceptibility data, shown in Fig. 2. The real part χ' of the complex ac susceptibility is plotted in Fig. 2(a), and is seen to show a sharp maximum at $T_c = 0.161(2) \text{ K}$. We first demonstrate that the value of χ' at T_c is of the order of the estimated limit $1/N_{\text{eff}}$ for a ferromagnetic powdered sample, where N_{eff} is an effective demagnetizing factor appropriate for the (cylindrically shaped) container filled with the grains. In the Appendix we argue that N_{eff} can be approximately given in terms of the demagnetizing factors N_{grain} and N_{cont} of, respectively, the individual grains and the container as [Eq. (A3)],

$$N_{\text{eff}} = N_{\text{grain}} + f(N_{\text{cont}} - 1/3), \quad (2)$$

where f denotes the volume filling fraction of the container.

Assuming the shape of the grains to be approximately spherical, we put $N_{\text{grain}} = 1/3$, while from the shape of the container, we estimate $N_{\text{cont}} \approx 0.2$. The density of the material is estimated to be $\rho_{\text{grain}} \approx 1.45 \text{ g/cm}^3$ from the value for the similar compound $\text{Mn}_6\text{O}_4\text{Br}_4(\text{Me}_2\text{dbm})_6$, and the filling fraction is estimated as $f \sim 1/3$. All this then leads to $N_{\text{eff}} \approx 0.29(5)$ and therefore $\chi'(T_c) \approx 1/N_{\text{eff}} = 3.5(6)$, the large error arising obviously from all the uncertainties in the above line of argument and in the estimates of the parameters involved. Next we should realize that this value would be valid for the χ' measured along the easy axis, whereas even a relatively small anisotropy will lower appreciably the χ' along the other directions.⁴⁰ Therefore, the powder χ' could

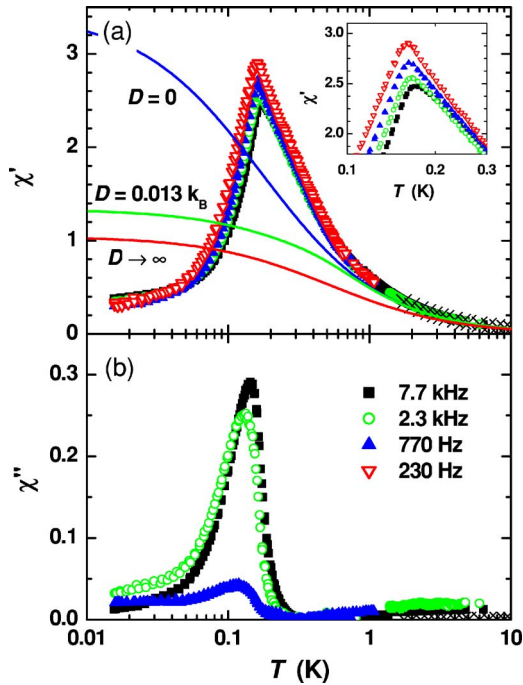


FIG. 2. (Color online) Real (a) and imaginary (b) components of the ac susceptibility at the indicated frequencies. Inset: magnification of $\chi'(T)$ to evidence the frequency dependence of the peak. The solid lines in panel (a) give the calculated behavior of the paramagnetic susceptibility (no interactions) for three values of the crystal field anisotropy constant D . In these calculations, the effect of the demagnetizing fields of the grains and the sample holder has been introduced as described in the Appendix.

easily be lower by a factor of 2 [see Eqs. (A5) and (A6) of the Appendix].

Given all the uncertainties, the above derived value can obviously serve as an order of magnitude estimate only, but we note that the experimental value of $\chi'(T_c) \approx 3$ is indeed rather close. Unfortunately, it proved to be impossible to obtain single crystals of the investigated compound, since measurements along the different crystallographic directions would have greatly facilitated the analysis. As a second argument for the ferromagnetic nature of the transition we include therefore in Fig. 2(a) the powder susceptibility expected for the paramagnetic (noninteracting) case, as calculated from the spin Hamiltonian [Eq. (1)] and applying in addition the corrections for demagnetizing effects as described in the Appendix. Besides the curve for $D/k_B = 0.013$ K appropriate for Mn_6 , we also include for comparison the fully isotropic ($D=0$) and infinite anisotropy limits. From this plot it is evident that, when approaching T_c , the susceptibility of Mn_6 increases appreciably above the paramagnetic limit, confirming the ferromagnetic nature of the correlations.

Below T_c , the powder χ' decreases rapidly, as expected for an anisotropic ferromagnet in which the domain-wall motions become progressively pinned. The associated domain-wall losses should then lead to a frequency dependent maximum around T_c in the imaginary part, χ'' , as the experimental data of Fig. 2(b) indeed show. In fact, although the Mn_6 spins can be considered as nearly isotropic at high temperatures,

the anisotropy energy is still large compared with the dipolar interaction energy $\mu_0\mu^2/4\pi k_B r^3 \approx 0.1$ K between nearest neighbor molecules. Thus the ordering should be that of an Ising dipolar ferromagnet.

As shown in detail in the inset of Fig. 2(a), the temperature T_{peak} at which the maximum value of χ' is found depends only weakly on ν , which we attribute to the anisotropy. The total activation energy for the reversal of each Mn_6 molecular spin amounts to $DS^2 \approx 1.9$ K, i.e., about 35 times smaller than for Mn_{12} . Although this is quite small, one could still expect the superparamagnetic blocking of the Mn_6 spins to occur when $T \approx T_B(\text{Mn}_{12})/35$, that is below ≈ 0.15 K. Since this value is very close to the actual T_c , one may expect that for $T \rightarrow T_c$ the approach to equilibrium begins to be hindered by the anisotropy of the individual molecular spins. We stress, however, that the frequency dependence of χ' observed here is quite different from that of the well-known anisotropic superparamagnetic clusters. A way to quantify the frequency dependence of the peak in χ' is by means of the parameter $\Delta T_{\text{peak}}/[T_{\text{peak}}\Delta(\log_{10} \nu)]$, which gives the variation of T_{peak} per decade of frequency. We find here $\Delta T_{\text{peak}}/[T_{\text{peak}}\Delta(\log_{10} \nu)] \approx 0.03-0.05$, to be compared with the typical values of ~ 0.20 for superparamagnetic blocking. In fact it is closer to the value ~ 0.06 found for certain types of spin glasses,⁴¹ but the peak observed here is much higher and sharper. Also, since the cluster spins are situated on a regular crystal lattice, a comparison with random magnetic systems would not be appropriate. The frequency dependence we observe is indeed very much weaker than is found in the $\text{LiHo}_x\text{Y}_{1-x}\text{F}_4$ system with $x=0.045$ (Ref. 42), for which x value that material is in the “antiglass” regime.^{43,44} In Mn_6 we found that $T_{\text{peak}}(\nu) \approx T_{\text{peak}}(0) + K\nu^\alpha$, with $\alpha \approx 0.4$ and a zero-frequency limit of the peak in $\chi'T_{\text{peak}}(0) \approx 158$ mK. At essentially the same temperature, we find a fairly sharp peak in the zero-field magnetic specific heat (see next section), instead of a broad anomaly as observed in $\text{LiHo}_{0.045}\text{Y}_{0.955}\text{F}_4$. Also this finding appears to exclude an interpretation in terms of a freezing transition in Mn_6 .

We finally turn to the susceptibility as measured above T_c in the paramagnetic region, which was plotted as $1/\chi'$ vs T in the inset of Fig. 2 in Ref. 29. We first note that no evidence for relaxation effects were found in this range. Up to a frequency of 7700 Hz no appreciable χ'' was detected and the measured χ' smoothly joins the data measured above 2 K with the SQUID susceptometer. We may therefore conclude that in the whole temperature range down to T_c the spin-lattice relaxation time is quite short, of the order 10^{-4} s or less.

The high-temperature susceptibility data χ'_i corrected for the demagnetizing field ($\chi'_i = \chi'/[1 - N_{\text{eff}}\chi']$) follow the Curie-Weiss law $\chi'_i = C/(T - \theta)$ quite well down to approximately 0.3 K, with $C = 0.62(2)$ K and $\theta = 0.14(3)$ K. The constant C equals, within the experimental errors, the theoretical value for isotropic spins $N_A g^2 \mu_0 \mu_B^2 S(S+1)/3k_B V_m = 0.595$ K, where $S=12$, $g=2$, and $V_m = 1647$ cm³/mole is the molar volume. The positive θ confirms the ferromagnetic nature of the ordered phase. The fact that mean field theory is so well obeyed down to very close to T_c is as expected for a

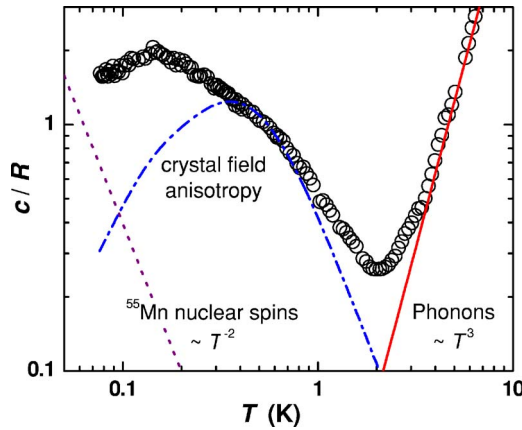


FIG. 3. (Color online) Zero-field specific heat of Mn_6 plotted as a function of temperature. Solid line: phonon contribution ($C/R=0.010 T^3$). Dashed-dotted line: Schottky contribution due to crystal field splitting of the $S=12$ multiplet as calculated with $D/k_B=0.013$ K. Dashed curve: expected nuclear contribution from the ^{55}Mn nuclear spins.

dipolar ferromagnet.^{45–48} We remark that the behavior of the powder susceptibility we observe for Mn_6 in Fig. 2 closely resembles previous powder data for $\text{Cs}_2\text{NaGdCl}_6$ (cf. Fig. 3 of Ref. 45) and $\text{LiHo}_x\text{Y}_{1-x}\text{F}_4$ ($x=0.46$) (cf. Fig. 1 in Ref. 49 and Fig. 4 in Ref. 42). Both materials are considered to be examples of anisotropic dipolar ferromagnets. Although weak ferromagnetism (i.e., canted antiferromagnetism) would also lead to $\chi(T=T_c)=1/N$, this would be accompanied by a negative Curie-Weiss θ , whereas we observe a positive value. Moreover, for canted antiferromagnetism an antisymmetric interaction term of the form $\mathbf{d}\cdot(\mathbf{S}_i\times\mathbf{S}_j)$ is needed (see, e.g., Ref. 50) and this is not expected for a system of equivalent magnetic moments interacting by dipolar interactions, as is the case here. For metamagnetic systems, having ferromagnetic nearest neighbor interactions and weaker further neighbor couplings, also a positive value for θ can be found but the magnetic ordering below T_c due to the further neighbor interaction is basically antiferromagnetic. Consequently, although the value of $\chi(T=T_c)$ can be much higher than for nearest neighbor antiferromagnets, it will fall still far below the ferromagnetic limit of $1/N$. We therefore conclude that the evidence for ferromagnetic dipolar order in Mn_6 presented here is quite strong. Additional studies, for instance of the spontaneous magnetization below T_c , would of course be welcome to provide further proof.

B. Zero-field specific heat

Specific heat data c taken in zero-applied field are shown in Fig. 3 as a function of temperature on a double logarithmic scale. Above 2 K, the specific heat is dominated by the contribution from the lattice phonons that can be reasonably fitted by the well-known low- T Debye approximation: $c_{\text{latt}}\propto(T/\Theta_D)^3$, with a Debye temperature $\Theta_D\approx 29$ K. Such low values are commonly observed in the molecular cluster compounds,^{5,15,28} reflecting the weak bonding between the cluster molecules in such molecular solids.

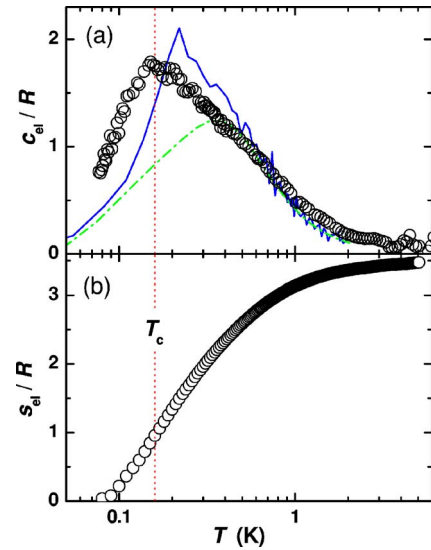


FIG. 4. (Color online) (a) T dependence of the electronic specific heat at zero applied field (circles). The dashed-dotted line is the Schottky anomaly calculated with $D/k_B=0.013$ K. The solid line is the Monte Carlo (MC) calculation for an orthorhombic lattice of 1024 Ising spins with periodic boundary conditions. For each point, 2×10^4 MC steps per spin were performed. (b) T dependence of the entropy obtained by integration of the electronic specific heat curve.

In the lowest temperature range below 0.1 K, the specific heat is seen to remain rather high valued, which can be mainly ascribed to the expected contribution from the ^{55}Mn nuclear spins, the energy levels of which are split by the hyperfine interaction with the Mn^{3+} electronic spins $s=2$ (see Sec. III D below). This contribution will become more clearly and directly visible in the field-dependent studies, where it will be shown to be describable by a term $c_{\text{nuc}}T^2/R\approx 5.2\times 10^{-3}\text{ K}^2$, which is plotted as the dashed line in Fig. 3. Anticipating the discussion below, we subtract this hyperfine contribution, as well as the phonon $\propto T^3$ term from the raw data in Fig. 3, in order to obtain the magnetic specific heat c_{el} associated with the cluster electron spin $S=12$ only, as plotted in Fig. 4. The resulting curve shows two characteristic features. At a temperature $T_c\approx 0.15(2)$ K a peak is observed, that can be associated with the transition to long-range magnetic order, in good agreement with the value for T_c deduced from the peak in the ac susceptibility extrapolated to zero frequency. Above T_c , one observes a widely extended “high-temperature tail,” that reflects the weak zero-field splittings (ZFS) of the $S=12$ multiplets by the crystal field interactions. We recall that even for a D value as small as 0.013 K the total splitting of an $S=12$ multiplet will still be an appreciable $DS^2=1.9$ K. In the absence of magnetic intercluster interactions the ZFS of such a multiplet would lead to a multilevel Schottky curve, shown as the dashed-dotted curve in both Figs. 3 and 4, where the fit to the experiment leads to the estimate $|D|/k_B\approx 0.013$ K, in reasonably good agreement with the values quoted above. In contrast with the highly anisotropic molecular clusters Mn_{12} , Mn_4 , and Fe_8 , where the multilevel ZFS Schottky is found above 1 K and is the most pronounced feature of the experi-

mentally observed magnetic specific heat,^{5,15,28} its presence in Mn_6 is masked at the low- T side by the ordering anomaly produced by the effects of the intercluster magnetic interactions. Numerical integration of c_{el}/T between 0.08 K and 4 K gives a total entropy change $\Delta s_{\text{el}}/R=3.5(2)$ per mole, close to the expected total entropy for a fully split $S=12$ multiplet, namely $\Delta s_{\text{el}}/R=\ln(2S+1)=3.22$. This confirms the consistency of the above subtraction procedure used to obtain c_{el} . The variation with temperature of the entropy, s_{el}/R , is also shown in Fig. 4. We note in particular that at T_c itself, the entropy only amounts to about $1R$ per mole, indicating that only the lowest energy levels of the cluster spins are involved in the actual magnetic ordering process, the majority of the higher-lying levels being already depopulated (the lowest lying doublet ground state on its own would already give a contribution to the entropy of $R \ln 2 = 0.69R$ per mole). Indeed, the distance to the nearest lying excited state would be equal to $(2S-1)D \approx 0.3$ K in the non-interacting limit.

C. Monte Carlo simulations

To simulate the zero-field specific heat data, Monte Carlo (MC) calculations were performed for an $S=12$ Ising model of magnetic dipoles on a body-centered orthorhombic lattice containing $Z=2$ molecules, with axes $a_x=15.7$ Å, $a_y=23.33$ Å, and $a_z=16.7$ Å. This choice approximates the crystal structure of $\text{Mn}_6\text{O}_4\text{Cl}_4(\text{Et}_2\text{dbm})_6$, that is the most closely related compound which yielded sufficiently large crystals for x-ray studies. To further simplify the Monte Carlo simulations, we approximated the monoclinic structure by an orthorhombic one. The density, $\rho=1.45$ g/cm³, was estimated from the $\text{Mn}_6\text{O}_4\text{Br}_4(\text{Me}_2\text{dbm})_6$ compound. The resulting molar volume is a few percent larger than what would be obtained from the lattice parameters used in the Monte Carlo simulation, but this discrepancy is due entirely to the approximation of orthorhombic structure. The Hamiltonian includes the dipolar interaction term as well as the anisotropy term $-DS_z^2$ given in Eq. (1). For $T < 0.5$ K the intermolecular dipolar interactions become important and remove the degeneracy of the $|\pm m\rangle$ spin doublets. The MC simulations show that the ground state is indeed ferromagnetically ordered, as observed, and predict a shape for c_{el} that is in good agreement with the experiment. In the upper panel of Fig. 4, we show c_{el} as calculated assuming all molecular easy (z) axes to point along a_z , i.e., one of the two nearly equivalent short axes of the actual lattice. Similar results were obtained for other orientations chosen for the anisotropy (z) axis. We note that our simulations give $T_c=0.22$ K, which is slightly higher than the experimental $T_c=0.161(2)$ K. This difference may be due to the Ising approximation taken for the intercluster dipolar interaction and to uncertainties in the values of the lattice parameters. In fact we note in passing that an almost perfect coincidence of our calculated curve with the experimental data may be obtained by assuming a smaller value of the magnetic moment, i.e., taking $g=1.75$ instead of $g=2.00$.

To pursue this point further, additional MC simulations were performed for the same crystal lattice, but now with

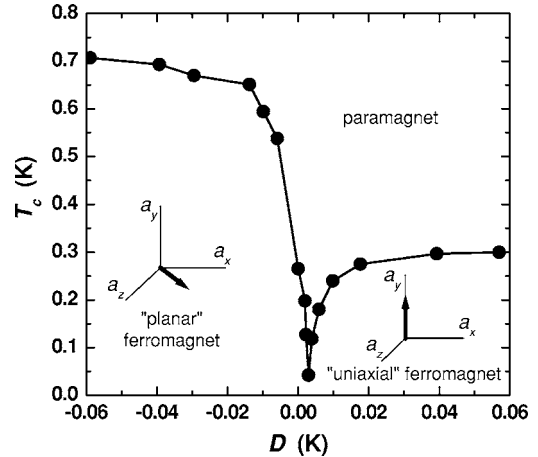


FIG. 5. Calculated critical temperature T_c as a function of the anisotropy parameter D , for classical Heisenberg spins.

classical Heisenberg spins replacing the $S=12$ Ising spins. To investigate the sensitivity of our results to the type of anisotropy, the sign and magnitude of D were varied. These calculations resulted in the phase diagram shown in Fig. 5, which we include here since it illustrates the complicated way in which the nature of the actual ground state and the value of T_c may depend on the combination of the long-range dipolar interaction and the anisotropy parameter. Although the ground state for this lattice is always found ferromagnetic, it can be either “uniaxial,” with strong preference for the spins to lie along the a_y axis [chosen for this particular example to be the anisotropy axis z of Eq. (1)], or “planar,” in the sense that the a_x - a_z plane becomes an easy plane, with a weak preference for a given direction in the plane, as sketched in the figure. Interestingly, the switching point between these “uniaxial” and “planar” orientations is not at $D=0$. The reason for this is as follows. Because the crystal lattice under consideration is far from being cubic, the dipolar interaction energy is rather anisotropic. The dipolar energy is minimized when the magnetization M points in the direction (in the a_x - a_z plane) shown in the inset on the left-hand side of Fig. 5. Therefore, M points along this direction for $D < 0$. On the other hand, the energy minimization for $D > 0$ is a competing process. Clearly, dipolar interaction must become dominant for sufficiently small values of D . The numerical results show that this occurs if $0 < D/k_B \lesssim 3$ mK. The numerical data points in Fig. 5 also show that T_c varies sharply within the $-0.01 < D/k_B < 0.01$ K range. System size effects and computer time restrictions do not allow us to determine whether T_c vanishes completely. The lowest numerical value obtained is as small as $T_c \approx 0.03$ K at $D/k_B \approx 3$ mK. Outside this narrow range of D , T_c is already almost equal to the limiting values of ≈ 0.7 K and ≈ 0.3 K, reached for infinite negative and positive D , respectively. Such a variation of T_c with anisotropy, as well as the form of the calculated and observed specific heat ordering anomaly, appear to be specific for dipolar interactions. They differ widely from the corresponding behavior known for three-dimensional (Heisenberg, Ising, XY) ferromagnetic lattices with nearest neighbor interaction only.⁵¹ For instance, in those models the variation of T_c with anisotropy is restricted

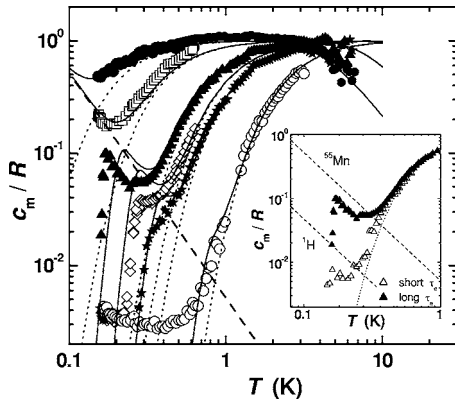


FIG. 6. Temperature dependence of the magnetic specific heat c_m at $B_a=0.5$ T (●), 1 T (□), 2 T (▲), 2.5 T (◇), 3 T (★), and 6 T (○). The dotted lines represent the calculated electronic contribution, whereas the dashed line is the expected nuclear specific heat at zero field calculated with Eq. (3). The solid lines represent the total time-dependent c_m (electronic+nuclear) calculated accounting for the nuclear T_{1n} (see text). Inset: detail of $c_m(T)$ at $B_a=2$ T, for long (~ 100 s) and short (~ 1 s) experimental times. The dashed lines are the calculated contributions arising from the ^{55}Mn and ^1H nuclear spins.

to about 20% of the T_c value, which moreover is highest for the Ising (“uniaxial”) case. It is also interesting to compare these Monte Carlo calculations with the predictions of simple mean field theory. The latter gives $T_c=2S^2J_{\text{eff}}/k_B$ and $T_c=2S(S+1)J_{\text{eff}}/3k_B$, respectively for $D\rightarrow+\infty$ and $D=0$, where J_{eff} is an effective interaction constant. The ratio between these two limits, which is $3S/(S+1)$, is about 2.5 times larger than what is obtained by Monte Carlo calculations.

In concluding this section we may stress that our detailed calculations have evidenced that for a dipolar magnet the value of T_c may vary strongly with anisotropy and lattice symmetry. This illustrates the danger in drawing conclusions about the nature of the magnetic interactions, i.e., whether they are of dipolar origin or not, just by comparing the value of $k_B T_c$ with the dipolar interaction energy of a pair of nearest neighboring spins. Our detailed calculations *specific* for this compound show a good quantitative agreement assuming just dipolar coupling, both as regards the value of T_c and the shape of the specific heat anomaly. Furthermore, the prediction that the ordering is ferromagnetic, as observed, is quite robust since it is independent of the details of the simulations. All this confirms that LRMO in Mn_6 is mainly driven by dipolar interactions.

D. Field-dependent specific heat: Nuclear spin contribution

We next discuss the time-dependent magnetic specific heat $c_m=c-c_{\text{latt}}$ measured under varying applied magnetic fields B_a , as plotted in Fig. 6. Even for the lowest B_a value, the ordering anomaly is already fully suppressed, as expected for a ferromagnet. Accordingly, we may account for these data with the Hamiltonian (1) neglecting dipolar interactions. The Zeeman term splits the otherwise degenerate $|\pm m\rangle$ doublets, and already for $B_a\sim 0.5$ T the level splittings become

predominantly determined by B_a , so that the anisotropy term can then also be neglected. As seen in Fig. 6, the calculations performed with $D=0$ (dotted curves) reproduce quite satisfactorily the data at higher temperatures.

However, when the maxima of the multilevel Schottky anomalies are shifted to higher T by increasing B_a , an additional contribution is revealed at low T . It is most clearly visible in the curves for $1\text{ T}<B<2.5\text{ T}$, and varies with temperature as $c_m T^2/R\approx 4\times 10^{-3}$. We attribute this contribution to the already-mentioned high-temperature tail of the equilibrium nuclear specific heat $c_{\text{nucl}}^{(\text{eq})}$. As discussed in Sec. IV, this specific heat should be dominated by the contributions of the six ^{55}Mn nuclear spins ($I=5/2$) and of the 114 protons present in each molecule. The energy levels of the former are split, even at zero field, by the strong on-site hyperfine interactions with the Mn^{3+} electronic spins $s=2$. For the specific heat analysis this interaction can be approximated by $\mathcal{H}_{\text{hf}}=A\mathbf{I}\cdot\mathbf{s}$, where A is an effective isotropic hyperfine coupling constant. By contrast, we may neglect the hyperfine splitting of the protons because it can be expected to be small compared to their nuclear Zeeman splitting for $B_a>1$ T. This is indeed confirmed by the NMR experiments shown below. The high-temperature limit of the nuclear specific heat can therefore be approximated by the sum of two contributions,⁵²

$$\frac{c_{\text{nucl}}^{(\text{eq})}T^2}{R}\approx 6\times\frac{1}{3}A^2s^2I(I+1)+114\times\left(\frac{\hbar\gamma_{\text{H}}B_a}{2k_B}\right)^2, \quad (3)$$

where $\gamma_{\text{H}}=2.675\times 10^8\text{ rad T}^{-1}\text{ s}^{-1}$ is the protons gyromagnetic ratio. Taking $A/k_B=8.6\text{ mK}$ as estimated from the NMR spectra measured for the same sample (see Sec. III E), we obtain the dashed line shown in Fig. 6 at zero field. This is the same contribution that was subtracted from the zero-field data shown in Fig. 4. The difference between the calculated and experimental $c_{\text{nucl}}^{(\text{eq})}$, which becomes especially evident for the $B_a=2$ T curve, can be due to the shift of the ^{55}Mn nuclear energy splittings by the applied field, which is neglected in Eq. (3).

A remarkable feature of the experimental data that is not reproduced by these equilibrium calculations is that, at the lowest T , the nuclear specific heat drops abruptly to a baseline of about $3\times 10^{-3}R$. This remaining specific heat is probably a background feature arising from incomplete correction for the field-dependent addenda contributions. The crossover temperature T^* where the drop of c_m occurs depends on B_a but also on the characteristic time constant τ_c of our (time-dependent) specific heat experiment: As is shown in the inset of Fig. 6, the deviation from the (calculated) equilibrium specific heat is found at a lower T when the system is given more time to relax. Interestingly, the specific heat becomes even smaller than the expected contribution of the protons. The drop therefore shows that, below T^* , the nuclear spins of both the ^1H and ^{55}Mn atoms cannot attain thermal equilibrium with the lattice phonons within the experimental time τ_c because the longitudinal nuclear spin-lattice relaxation time becomes too short. This relaxation effect can be described as follows:

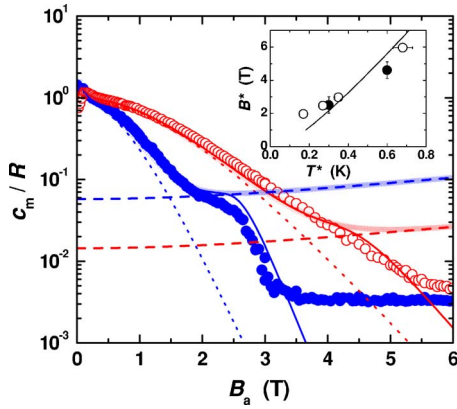


FIG. 7. (Color online) Field dependence of the magnetic specific heat at $T=0.3$ K (solid dots) and $T=0.6$ K (open dots). The dashed and dotted lines represent respectively the calculated nuclear [see Eq. (3)] and electronic contributions to the equilibrium specific heat. The thick and thin solid lines give respectively the equilibrium c_m and the time-dependent c_m calculated accounting for the field-dependent nuclear T_{1n} . Inset: $B^*(T^*)$ obtained from T sweeps, as in Fig. 6 (open dots), or from B -sweeps, as in the present figure (solid dots). From the fit (solid line) to Eq. (5) we extract $\kappa_0 \approx 40 \text{ s}^{-1} \text{ T}^{-3}$.

$$c_{\text{nucl}}(\tau_e) = c_{\text{nucl}}^{(\text{eq})} [1 - \exp(-\tau_e/T_{1n})], \quad (4)$$

where, to simplify the discussion, we have used the same nuclear spin-lattice relaxation (NSLR) time T_{1n} for both protons and ^{55}Mn although they can obviously differ from each other. According to Eq. (4) the specific heat decreases fast when T_{1n} becomes of the order of τ_e . This crossover to a nonequilibrium regime (as measured by time-dependent specific heat) provides therefore direct information on the temperature and field dependence of the nuclear T_{1n} .

As is well established,⁵³ $T_{1n}(T, B_a)$ can be related to the time-dependent part of the transverse hyperfine field as produced by the fluctuations of the electron spin. For the case of Mn_6 both the electron spin fluctuations due to spin-lattice coupling and to dipolar spin-spin interactions will have to be considered. A more extensive theoretical treatment is given below in Sec. IV, in terms of existing models for nuclear relaxation in magnetic crystals. As will be seen, this treatment predicts the behavior of the longitudinal nuclear spin-lattice relaxation time at low temperature and high fields (>3 T) to be given by

$$\frac{1}{T_{1n}} \approx \kappa_0 B_a^3 \exp\left(-\frac{g\mu_B B_a}{k_B T}\right), \quad (5)$$

where κ_0 is a constant that depends on the electronic spin-lattice relaxation rate and on the details of the relaxation mechanism. This shows that an exponential temperature dependence of the NSLR rate is expected at high fields. The effect of the field is to polarize the electron spins, which reduces the fluctuations of the hyperfine field, thus effectively disconnecting the nuclear spins from the lattice.

As seen from Eq. (5) the nuclear spins can be taken out of equilibrium either by decreasing T down to T^* at constant field (as in Fig. 6), or by increasing B_a up to a given value B^*

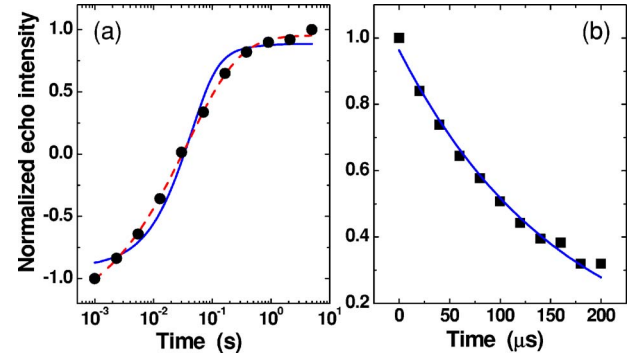


FIG. 8. (Color online) Inversion recovery (a) and decay of transverse magnetization (b) for the ^{55}Mn nuclei at $T=0.9$ K, $B_a=5$ T, and $\nu=251.5$ MHz. The lines in (a) are fits to Eq. (6) with $\alpha \approx 0.5$ (dashed) and $\alpha=1$ (solid). The solid line in (b) is a fit to Eq. (7).

at constant T . The latter effect is indeed also observed experimentally, as shown in Fig. 7 for $T=0.3$ K and 0.6 K. In this figure the transition to nonequilibrium is obvious from the fact that the data measured in high field fall far below the expected nuclear contributions (dashed lines). The inset of Fig. 7 shows $B^*(T^*)$ obtained either from T sweeps at constant B (as in Fig. 6) or from B sweeps at constant T (as in Fig. 7). The two methods prove to be fully consistent with each other. The fit of $B^*(T^*)$ using Eq. (5) gives an average value of $\kappa_0 \approx 40 \text{ s}^{-1} \text{ T}^{-3}$. Using this value of κ_0 we have calculated the time-dependent c_{nucl} from Eq. (4). Adding this to the calculated electronic specific heat yields the solid lines in Figs. 6 and 7, which can be seen to be in reasonably good agreement with the experimental data over the whole range of field and temperature.

E. ^{55}Mn NMR and nuclear relaxation

The nuclear spin-lattice relaxation in Mn_6 has been further investigated by ^{55}Mn nuclear magnetic resonance. Apart from the fundamental question as to by which mechanisms the magnetic relaxation proceeds in this isotropic molecular magnetic crystal, it is of interest to compare with the typical behavior observed recently for the highly anisotropic single-molecule magnets like $\text{Mn}_{12}\text{-ac}$.^{34–36}

As is well known, it is difficult to observe NMR for nuclei of paramagnetic ions due to the very large and strongly fluctuating magnetic fields produced at the nuclei by the electron spin through the (on-site) hyperfine interactions. As a consequence, nuclear resonance lines become very broad and spin-lattice relaxation rates too fast to be measured. To enable the observation of the NMR signals, one should therefore take recourse to the low-temperature and high-field regime, in which electron spin fluctuations can be expected to be sufficiently suppressed. Accordingly, we performed our experiments at $T=0.9$ K, using a ^3He cryostat, and fields in the range 3 to 7 T.

The ^{55}Mn NSLR was studied by measuring the recovery of the nuclear magnetization after an inversion pulse. By integrating the echo intensity we obtained recovery curves as those shown in Fig. 8(a). For the ease of comparison be-

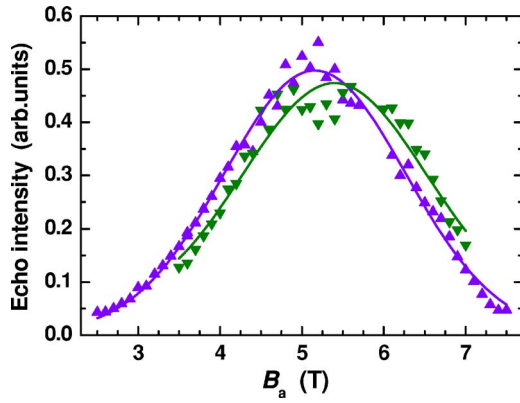


FIG. 9. (Color online) ^{55}Mn NMR spectra at $T=0.9$ K and measuring frequencies $\nu=246.5$ MHz (down triangles) and $\nu=251.5$ MHz (up triangles). The gap in the data around $B_a \approx 5.8$ T is due to the crossing with the ^1H line arising from the Zeeman-split proton levels. The lines are Gaussian fits with total width $2\sigma_B \approx 2.2$ T.

tween different curves, we renormalize the vertical scale such that $M(0)/M(\infty)=-1$ and $M(t \gg T_{1n})/M(\infty)=1$, even though usually $|M(0)| < |M(\infty)|$: this is just an artifact that occurs when the NMR line is much broader than the spectrum of the inversion pulse, and does not mean that the length of the π pulse is incorrect. Since the ^{55}Mn nuclei have spin $I=5/2$, the recovery of the nuclear relaxation for the central line in the quadrupolar split manifold is described by⁵⁴

$$\frac{M(t)}{M(\infty)} = 1 - \left[\frac{100}{63} e^{-(15t/T_{1n})^\alpha} + \frac{16}{45} e^{-(6t/T_{1n})^\alpha} + \frac{2}{35} e^{-(t/T_{1n})^\alpha} \right], \quad (6)$$

where $1/T_{1n}$ is the nuclear spin-lattice relaxation rate, and α is a stretching exponent, which needs to be introduced to account for the large inhomogeneity of the NMR line, which causes the inversion recovery to consist of a combination of recoveries with different rates. We typically found an optimal value of $\alpha \approx 0.5$, although the choice of the stretching exponent does not strongly influence the value of $1/T_{1n}$ extracted from the fit.

The transverse spin-spin relaxation (TSSR) rate $1/T_{2n}$ was studied by measuring the decay of echo intensity upon increasing the waiting time τ between the $\pi/2$ and the π pulses. The decay of transverse magnetization $M_\perp(\tau)$ can be fitted to a single exponential

$$\frac{M_\perp(2\tau)}{M_\perp(0)} = e^{-2\tau/T_{2n}}, \quad (7)$$

as shown in Fig. 8(b).

The field-sweep NMR spectra in Fig. 9 clearly show that it is impossible to determine whether there are inequivalent sites in the molecule, as regards the hyperfine coupling [compare with the case of $\text{Mn}_{12}\text{-ac}$ (Ref. 55)]. This may be due to the large quadrupolar splitting expected in Mn^{3+} sites, plus the fact that our sample is an unoriented powder. As expected from the internal ferromagnetic structure of the

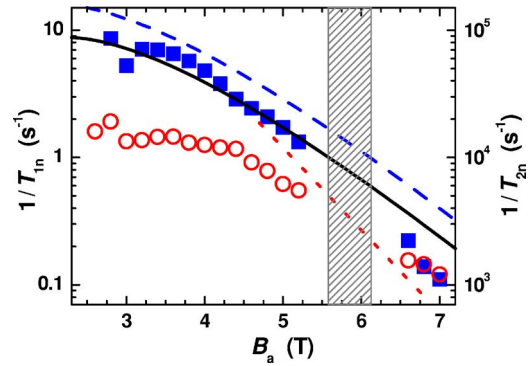


FIG. 10. (Color online) Field dependencies of the ^{55}Mn NSLR (full squares, left scale) and TSSR (open circles, right scale) at $T=0.9$ K and $\nu=251.5$ MHz. Notice the factor 10^4 between left and right scales. The hatched area around 5.8 T indicates the region where the ^1H line overlaps with the ^{55}Mn resonance. Dashed line: calculated $1/T_{1n}(B_a)$ according to Eq. (5) for the value $\kappa_0=40 \text{ s}^{-1} \text{ T}^{-3}$ as extracted from specific heat experiments. This represents exactly the same line as in the inset of Fig. 7. Solid line: fit to Eq. (34) below with parameters discussed in the text. Dotted line: $1/T_{2n}$ calculated according to Eq. (25).

cluster electron spins, the ^{55}Mn spectrum shifts to higher fields when lowering the frequency. The spectra can be fitted by a Gaussian shape with total width $2\sigma_B \approx 2.2$ T. If this width were due to quadrupolar splitting $\Delta\nu_Q$ only, one would deduce $\Delta\nu_Q \sim 7$ MHz: this estimate can be obtained from a comparison to the $\text{Mn}^{(1)}$ line in $\text{Mn}_{12}\text{-ac}$, where $\Delta\nu_Q = 0.72$ MHz yields $2\sigma_v = 2.4$ MHz,⁵⁵ i.e., $2\sigma_B = 2\sigma_v / (\gamma_{\text{Mn}}/2\pi) \approx 0.23$ T, where $\gamma_{\text{Mn}} = 6.64 \times 10^7 \text{ rad T}^{-1} \text{ s}^{-1}$ is the ^{55}Mn gyromagnetic ratio. Such an estimate is thus even larger than the highest $\Delta\nu_Q \approx 4.3$ MHz found in the $\text{Mn}^{(2)}$ sites of the less symmetric $\text{Mn}_{12}\text{-ac}$ cluster.⁵⁵ We expect therefore that the random orientation of the crystallites and, eventually, the presence of inequivalent Mn sites as regards the hyperfine coupling, are also contributing to the observed broadening. Indeed, when decreasing the frequency by 5 MHz the maximum of the spectrum shifts only by 0.24 T, instead of the 0.47 T that would be expected when all the local hyperfine fields are antiparallel to B_a . We conclude that the observed spectrum, as well as the NSLR and TSSR data, should be considered as obtained from a mixture of nuclear signals arising from randomly oriented crystallites with largely overlapping and quadrupolar-split NMR lines from all the Mn sites in the cluster. Extrapolating to $B_a=0$ the field dependence of the peak of the spectrum, one obtains $\nu(0) \approx 360 \text{ MHz} \Rightarrow B_{\text{hyp}} \approx 34$ T, very similar to the highest value found in the $\text{Mn}^{(3)}$ site of $\text{Mn}_{12}\text{-ac}$.⁵⁵ Finally, in connection with the discussion of the nuclear specific heat of the previous section, it is interesting to mention that the ^1H resonance is found at a value of field given simply by $B_H \approx \omega / \gamma_H$ (the excluded region in the spectra shown in Fig. 9). This confirms that the local hyperfine fields do not appreciably shift the ^1H resonance frequency and, therefore, for sufficiently high fields ($B_a > 1$ T), the hyperfine interaction of protons can be neglected, as we did.

Figure 10 shows the field dependencies of the NSLR rate $1/T_{1n}$ and the TSSR rate $1/T_{2n}$, measured at constant fre-

quency $\nu=251.5$ MHz and temperature $T=0.9$ K. From the discussion above it is clear that these data must be interpreted with a certain caution, since shifting B_a at constant ν means that we are sampling each time a different portion of the NMR signal, which means different quadrupolar satellites, different orientation of the crystallites, etc. Nevertheless, the agreement with the estimate of T_{1n} obtained by specific heat data (inset of Fig. 6) turns out to be satisfactory. We can directly compare the NSLR rates $1/T_{1n}(B_a)$ obtained from respectively NMR and specific heat data by plotting (dashed line in Fig. 10) $1/T_{1n}(B_a)$ as calculated from Eq. (5), with $T=0.9$ K and fixing $\kappa_0=40$ s⁻¹ T⁻³ as obtained from the fit of $B^*(T^*)$ in the inset of Fig. 7. The agreement is seen to be reasonable. The solid line in the same figure represents a fit to the $1/T_{1n}(B_a)$ based on a model described by Eq. (34) of the following section, with parameters given in the discussion there.

In Fig. 10 we also show the TSSR rate $1/T_{2n}(B_a)$, with ordinate axis shifted in order to compare its field dependence to that found for the NSLR rate. As explained below, we expect $1/T_{2n}(B_a) \propto \exp(g\mu_B B_a/k_B T)$ at high fields. This dependence, and the quantitative result calculated according to Eq. (25), are shown as a dotted line in Fig. 10 and yield the right order of magnitude of the observed $T_{2n} \approx 0.1-1$ ms.

IV. DISCUSSION: MAGNETIC HYPERFINE INTERACTIONS AND NUCLEAR MAGNETIC RELAXATION

In this section we apply theoretical results for magnetic hyperfine interactions and nuclear magnetic relaxation in magnetic insulating solids to interpret the data of the previous sections. We recall that for such materials direct relaxation channels such as quadrupolar interactions connecting nuclear spins to the lattice become ineffective at low temperatures. Thus the electron spins present have to serve as an intermediary between nuclei and phonons in some way or the other and we have to consider the interconnected spin dynamics of both nuclear and electron spin systems and their coupling to the lattice. As will be shown below, for highly polarized electron spin systems, such as Mn₆ in high fields at low temperature, the relaxation behavior can be adequately described in terms of theoretical models previously developed in the field of dynamic nuclear polarization. These same models should also provide a good basis to describe the relaxation in highly anisotropic single-molecule magnets like Mn₁₂-ac and Fe₈ below their blocking temperatures, where an extreme polarization of the electron spins is induced by the crystal field. Although several groups have described the application to molecular magnets of some general theories of nuclear relaxation,^{35,56-58} it appears that the role of the electronic dipolar coupling has so far been overlooked. We therefore consider worthwhile to give a detailed overview of the different ingredients needed to arrive at a consistent picture describing the behavior we observe in both the NMR and the specific heat of Mn₆, being confident it will be quite useful for the other materials mentioned as well. We will briefly come back to this point in the conclusion section, drawing a comparison with our observations in Mn₁₂-ac. We start with

an evaluation of the relevant hyperfine interactions between the cluster spins and the various nuclear spins in the Mn₆ molecular cluster. Quite generally,^{53,59} the hyperfine interaction Hamiltonian of a nuclear moment \mathbf{I} with the surrounding electron spins \mathbf{s}_j can be written in the form of the bilinear coupling

$$\mathcal{H}_{\text{hf}} = \sum_j \mathbf{I} \cdot \tilde{\mathbf{A}} \cdot \mathbf{s}_j. \quad (8)$$

Here the hyperfine interaction $\tilde{\mathbf{A}}$ is a second rank tensor and summation is over electron spins on both the same atom and surrounding atoms. It is often convenient to interpret the hyperfine coupling in terms of a magnetic hyperfine field: $B_{\text{hf}} = -(\gamma_n \hbar)^{-1} \mathbf{s} \cdot \tilde{\mathbf{A}}$, acting on the nuclear spin in addition to the applied field B_a . γ_n is the nuclear gyromagnetic ratio. The total magnetic Hamiltonian for the nuclear spins then becomes

$$\mathcal{H}_{\text{hf}} = -\gamma_n \hbar \mathbf{I} \cdot (\mathbf{B}_a + \mathbf{B}_{\text{hf}}) = -\gamma_n \hbar \mathbf{I} \cdot \mathbf{B}_{\text{tot}}. \quad (9)$$

In principle \mathcal{H}_{hf} will be time dependent since both $\tilde{\mathbf{A}}$ and \mathbf{s}_j can depend on time due to, respectively, atomic motions (not considered here) and fluctuations of the electron spins. Provided that the frequency of these fluctuations is fast compared to the nuclear Larmor frequencies produced in the static case, the nuclear resonance is still well defined by it at a frequency that is shifted with respect to that for $\mathbf{B}_{\text{hf}}=0$, the shift being proportional to the time average of $\tilde{\mathbf{A}}(t) \cdot \mathbf{s}$. In the effective field picture the hyperfine field can be split up into a static part, $\langle \mathbf{B}_{\text{hf}} \rangle$, and a time-dependent part $\mathbf{B}_{\text{hf}}(t) = \langle \mathbf{B}_{\text{hf}} \rangle + \mathbf{b}(t)$. The time-dependent fraction, $\mathbf{b}(t)$, is usually much smaller and can then be treated as a perturbation that may produce relaxation of the nuclear polarization. Neglecting the quadrupolar interactions, the remaining magnetic hyperfine interaction may be decomposed into contributions coming from the coupling of the nuclear moment with the orbital motions of the electrons, the dipolar interactions with the electron spins and, in case a finite density of electrons is present at the nuclear site, the part due to the Fermi-contact interaction. Thus we may write $\langle \mathbf{B}_{\text{hf}} \rangle = \mathbf{B}_{\text{dip}} + \mathbf{B}_L + \mathbf{B}_F$, in an obvious notation. As for the relative strengths of these contributions, for nuclei (such as the present ⁵⁵Mn) residing on magnetic atoms the Fermi-contact term is strongest by far, with $B_F \sim 10-10^2$ T, followed by the orbital and dipolar interactions with electrons on the same atom (on site), typically of order 10 T. For ions with closed or half-filled shells both B_L and B_{dip} vanish, whereas also for non-*S*-state ions, such as Mn³⁺, the orbital moment can be quenched by crystal-field splittings, so that B_L becomes negligible. Furthermore, nuclei on nonmagnetic ligand atoms directly coordinating the magnetic ions via covalent bonds may also experience substantial Fermi-contact interaction, of order 1-10 T. Nuclei on more distant nonmagnetic atoms will mainly experience the long-range dipolar interactions, giving typically $B_{\text{dip}} \sim 0.1-1$ T.

For the ⁵⁵Mn nuclei on the Mn³⁺ ions (with nuclear spin $I=5/2$ and electron spin $s=2$) of the present compound Mn₆ we deduced in Sec. III E a resonance frequency (extrapolated

to $B_a=0$) centered around 360 MHz (corresponding to $\langle B_{\text{hf}} \rangle = 34$ T), which is almost the same as the value 364 MHz Kubo *et al.*⁵⁵ recently found for one of the two Mn^{3+} sites in $\text{Mn}_{12}\text{-ac}$. According to their analysis, the corresponding $B_{\text{hf}} = 34.5$ T for this site results from the combination of Fermi-contact and dipolar fields $B_F=41$ T and $B_{\text{dip}}=14$ T that are of opposite sign. As they point out, the value for B_F should not vary much for the same ion in comparable coordinations, quoting values for Mn^{3+} in TiO_2 and in MnFe_2O_4 of, respectively, $B_F=42$ T and 36 T (with $B_{\text{dip}}=12$ T and 11.5 T, again of opposite sign). We may therefore assume similar values for these fields in Mn_6 . As is often done, in order to estimate the resulting nuclear energy level splittings responsible for the measured hyperfine specific heat, we have in Secs. III B and III D approximated the net time average of the diagonal part of the (slightly anisotropic⁵⁵) hyperfine interaction by an effective isotropic scalar interaction $\mathcal{H}_{\text{hf, is}} = A\mathbf{s} \cdot \mathbf{I}$, where $A = -\gamma_n \hbar B_{\text{hf}}/s$, $s=2$ and $A/k_B = 8.7$ mK (corresponding to $B_{\text{hf}}=34$ T). As for the other nuclei present in Mn_6 , the only sizable contribution to be expected is that arising from the long-range dipolar interactions of the proton spins with the surrounding electronic spins. Since these dipolar fields are small, their contribution may be neglected in zero-applied field as compared to that of the ^{55}Mn nuclei, and only becomes substantial for applied fields exceeding 1 T. Although transferred hyperfine interactions with nuclei on the oxygen and Br ions that are directly bonded covalently to the Mn atoms could be substantial,⁵⁵ we may nevertheless neglect their contributions in comparison with the other ones in view of the low abundance of the ^{17}O isotope and the low number of Br atoms present.

Considering next the nuclear spin relaxation (NSR) we remark that the longitudinal NSR rate, $1/T_{1n}$, is given quite generally by the expression

$$\frac{1}{T_{1n}} = \frac{1}{2} \sum_{m,n} W_{m,n} (E_m - E_n)^2 \bigg/ \sum_m E_m^2, \quad (10)$$

where $W_{m,n}$ denotes the probability for a transition between nuclear energy levels m, n induced by the perturbation considered. As mentioned, we assume the main source for NSR to be the time-dependent fluctuations of the electron spins $\mathbf{s}(t)$ that produce fluctuating components $\mathbf{b}(t)$ of the hyperfine field. The theory has been developed by Moriya,^{60–62} on basis of the general theory of magnetic resonance absorption of Kubo and Tomita.⁶³ Two possible sources for the electron spin fluctuations have to be considered, namely electron spin-lattice relaxation, characterized by the longitudinal electron spin-lattice relaxation rate $1/T_{1e}$, and spin-spin relaxation, due to magnetic interactions (dipolar or exchange) between the electron spins and characterized by the transverse electron spin-relaxation rate $1/T_{2e}$. Obviously, hyperfine interaction terms producing NSR should involve operator combinations as $I^{\pm} s^z$, $I^+ s^-$ and $I^- s^+$, $I^+ s^+$ and $I^- s^-$. The first of these distinguishes itself in that a nuclear spin flip is *not* combined with an electronic spin flip. It follows that this first type involves transitions at NMR frequencies $\omega = \omega_n$, the others at ESR frequencies $\omega = \omega_e \pm \omega_n \approx \omega_e$. In the high- T approximation, the NSR rate can be expressed in terms of the

spectral densities f_j^α of the two-spin ($i \neq j$) and autocorrelation ($i=j$) functions $\langle s_i^\alpha(0) s_j^\alpha(t) \rangle$ at these frequencies as

$$\frac{1}{T_{1n}} = \frac{2}{3} s(s+1) \sum_j [A_j f_j^z(\omega_n) + B_j f_j^z(\omega_e)], \quad (11)$$

$$f_j^\alpha(\omega) = \int_{-\infty}^{+\infty} \langle s_i^\alpha(0) s_j^\alpha(t) \rangle e^{-i\omega t} dt \quad (\alpha = \pm, z). \quad (12)$$

The coefficients A_j and B_j are constants depending on the details of the hyperfine interactions. For the ease of discussion we approximate the Fermi-contact interaction by an isotropic scalar on-site hyperfine coupling and neglect possible orbital contributions. Adding the dipolar interaction, the hyperfine Hamiltonian becomes:

$$\mathcal{H}_{\text{hf}} = A \mathbf{I}_i \cdot \mathbf{s}_i + \frac{\mu_0}{4\pi} \gamma_e \gamma_n \hbar^2 \sum_j \left[\frac{\mathbf{I}_i \cdot \mathbf{s}_j}{r_{ij}^3} - 3 \frac{(\mathbf{I}_i \cdot \mathbf{r}_{ij})(\mathbf{s}_j \cdot \mathbf{r}_{ij})}{r_{ij}^5} \right], \quad (13)$$

where γ_e is the electronic gyromagnetic ratio. For the terms responsible for NSR one then obtains

$$\mathcal{H}' = I_i^+ \sum_j D_{ij}^z s_j^z(t) + I_i^+ \left[(1/2) A s_i^- + \sum_j (D_{ij}^- s_j^- + D_{ij}^+ s_j^+) \right] + \text{c.c.}, \quad (14)$$

where D_{ij}^z and D_{ij}^\pm denote the components of the dipolar coupling tensor connecting I_i^+ with s_j^z and with s_j^\pm , respectively, and c.c. stands for complex conjugates. It is important to note that for a pure scalar hyperfine interaction only the transverse spectral densities $f_j^\pm(\omega_e)$ do appear. Assuming an exponential decay of the spin-correlation functions, the scalar interaction leads to the NSR rate⁵³

$$\frac{1}{T_{1n}} = \frac{1}{2} A^2 \int_{-\infty}^{+\infty} \langle s^+(0) s^-(t) \rangle e^{i(\omega_e - \omega_n)t} dt = \frac{1}{3} s(s+1) A^2 \frac{T_{2e}}{1 + (\omega_e - \omega_n)^2 T_{2e}^2}. \quad (15)$$

As noted above, relaxation then requires energies $\hbar \omega_e$ of the order of the electronic level splittings. By contrast the dipolar interaction contains terms of different symmetry,^{53,59} so that it contributes to both transverse and longitudinal terms. In particular it contains the operator $D_{ij}^z \propto -(3/2) \sin \theta \cos \theta e^{-i\phi}$ that may induce a nuclear flip unaccompanied by an electron flip, thus involving the much smaller energy $\hbar \omega_n$. The NSR rate due to this process, after averaging over the angular dependence, is obtained as⁵³

$$\frac{1}{T_{1n}} = \frac{3}{5} \left(\frac{\mu_0}{4\pi} \right)^2 (\gamma_e \gamma_n \hbar)^2 r^{-6} \int_{-\infty}^{+\infty} \langle s^z(0) s^z(t) \rangle e^{-i\omega_n t} dt. \quad (16)$$

Considering now first the case that the electron spin fluctuations arise from electron spin-lattice relaxation, and assuming again an exponential decay of the autocorrelation function, in this case with longitudinal relaxation rate $1/T_{1e}$,

$$\langle s^z(0)s^z(t) \rangle = \frac{1}{3}s(s+1)\exp(-t/T_{1e}), \quad (17)$$

the NSR rate by this process is found to be given by

$$\frac{1}{T_{1n}^{(EZ)}} = \frac{2}{5} \left(\frac{\mu_0}{4\pi} \right)^2 (\gamma_e \gamma_n \hbar)^2 r^{-6} s(s+1) \frac{T_{1e}}{1 + \omega_n^2 T_{1e}^2}, \quad (18)$$

an expression first derived by Bloembergen⁶⁴ for the nuclear spin-lattice relaxation by paramagnetic impurities in diamagnetic crystals. The superscript (EZ) is added to indicate that this nuclear relaxation is driven by the spin-lattice relaxation of the electron-Zeeman reservoir. Comparing Eqs. (15) and (18) it is clear that, unless the electronic linewidths would be comparable to the level splittings ω_e , the latter process will outweigh the previous one by the large factor $(\omega_e/\omega_n)^2$. In most cases of interest one further has $\omega_n T_{1e} \gg 1$, so that one may write approximately

$$\frac{1}{T_{1n}^{(EZ)}} \approx \frac{2}{5} \left(\frac{\mu_0}{4\pi} \right)^2 \frac{(\gamma_e \gamma_n \hbar)^2 r^{-6} s(s+1)}{\omega_n^2 T_{1e}} = \frac{2}{5} \left(\frac{B_{\text{dip}}}{B_{\text{tot}}} \right)^2 \frac{1}{T_{1e}}. \quad (19)$$

Here $B_{\text{dip}} = (\mu_0/4\pi)\hbar\gamma_e\sqrt{s(s+1)}r^{-3}$ stands for the electronic dipolar field at the nuclear site, and $B_{\text{tot}} = B_a + B_{\text{hf}} = \omega_n/\gamma_n$ is the total field responsible for the nuclear Zeeman splittings.⁵³

In the next step we have to compare this result with the NSR rate arising from spin-spin interactions, which for Mn_6 amount to the dipolar interactions between the electronic cluster spins $S=12$. We note that since the total spin $S=12$ of the Mn_6 cluster results from the strong ferromagnetic intramolecular exchange between the atomic spins $s=2$, the fluctuations of the total spin are obviously related to those of the constituting atomic spins and vice versa. Thus, although both the hyperfine interactions and the electron spin lattice coupling basically involve the atomic spins, the atomic spin fluctuations nevertheless are in a one-to-one relationship with those of the cluster spins. Due to such spin-spin interactions the spectral density will no longer be given by a Lorentzian. Instead of the exponential decay of the correlation functions, Eq. (17), one usually assumes a Gaussian approximation for the autocorrelation functions,⁶⁰⁻⁶²

$$\langle s^z(0)s^z(t) \rangle = \frac{1}{2} \langle s^+(0)s^-(t) \rangle = \frac{1}{3}s(s+1)\exp(-\omega_{\text{int}}^2 t^2). \quad (20)$$

For the longitudinal NSR rate one obtains

$$\frac{1}{T_{1n}^{(\text{ED})}} = \frac{\sqrt{2\pi}}{3} \gamma_n^2 B_{\text{dip}}^2 \omega_{\text{int}}^{-1} \exp(-\omega_n^2/2\omega_{\text{int}}^2), \quad (21)$$

where (ED) indicates that this process is driven by fluctuations in the electron-dipolar reservoir. For the transverse relaxation one finds similarly

$$\frac{1}{T_{2n}} = \frac{1}{2T_{1n}^{(\text{ED})}} [1 + \exp(-\omega_n^2/2\omega_{\text{int}}^2)], \quad (22)$$

from which it follows that $1/T_{2n} \approx 1/T_{1n}^{(\text{ED})}$. Here ω_{int} stands for the electronic dipolar spin-spin interaction,⁶⁵ which in

our case can be estimated from the dipolar ordering temperature, $\hbar\omega_{\text{int}} \approx k_B T_c$, and also corresponds to the electronic TSSR rate, $\omega_{\text{int}} \approx 1/T_{2e}$.

At this point it is important to emphasize that the above derivations are essentially only valid at high temperatures and low applied fields, since the effects of polarization of the electronic spins by the applied field have been neglected. As noted already by Moriya⁶¹ and in later work on dynamic polarization,^{66,67} the more the electron spins become polarized, the less they will be able to relax the nuclear spins. To account for this, one should replace the time dependencies of the electronic spin $\mathbf{s}(t)$ by its fluctuating part, $\delta\mathbf{s}(t) = \mathbf{s}(t) - \mathbf{s}_0$, where \mathbf{s}_0 denotes the thermal average of \mathbf{s} . Thus, instead of an expression as in Eq. (17) for the decay of the electronic spin, one should take⁶¹

$$\begin{aligned} \langle \delta s^z(0) \delta s^z(t) \rangle &= \langle [s^z(0) - \bar{s}_0^z][s^z(t) - \bar{s}_0^z] \rangle \\ &= \langle (s^z - \bar{s}_0^z)^2 \rangle \exp(-t/T_{1e}) \\ &= S(\partial/\partial X) \bar{s}_0^z(X) \exp(-t/T_{1e}) \\ &= Ss(\partial/\partial X) B_S(X) \exp(-t/T_{1e}), \end{aligned} \quad (23)$$

using the fact that the thermal average of each Mn^{3+} spin s^z is given by $sB_S(X)$, where $X = g\mu_B B_a/k_B T$, $s=2$, and B_S is the Brillouin function for the *total* molecular spin S . Accordingly, the expression (17) for the electron spin autocorrelation function should be multiplied by the factor $3S(s+1)^{-1} \partial B_S/\partial X$. Restricting in what follows to the simplest case of spin $S=1/2$, as appropriate for the present experiments in the high-field/low- T range where only the two lowest lying electron Zeeman states are relevant, this factor reduces to $(1 - \tanh^2 X)/2$, with $X = g\mu_B B_a/2k_B T$. We thus obtain for $1/T_{1n}^{(\text{EZ})}$ instead of Eq. (19) the relation

$$\frac{1}{T_{1n}^{(\text{EZ})}} \approx \frac{1}{5} \left(\frac{B_{\text{dip}}}{B_{\text{tot}}} \right)^2 (1 - \tanh^2 X) \frac{1}{T_{1e}}, \quad (24)$$

whereas instead of Eq. (21) one has now

$$\frac{1}{T_{1n}^{(\text{ED})}} \approx \frac{1}{T_{2n}^{(\text{ED})}} \approx \frac{\sqrt{2\pi}}{6} \frac{(\gamma_n B_{\text{dip}})^2}{\omega_{\text{int}}} (1 - \tanh^2 X) \exp(-\omega_n^2/2\omega_{\text{int}}^2). \quad (25)$$

In both cases, since $\tanh X$ gives the degree of polarization of the electron spin, one observes that when this approaches unity the nuclear relaxation rate goes to zero, as to be expected. For the electron-dipolar relaxation channel one should notice that, although the actual electronic linewidth $1/T_{2e}$ strongly depends on the electronic polarization (the second moment of the absorption line is proportional to $1 - \tanh^2 X$, cf. Ref. 52), ω_{int} in (25) is still given by the dipolar coupling as calculated in the high- T limit.⁶⁵

Proceeding next to compare the above predictions with the high-field NMR experiment, we may already notice that Eq. (25) yields the right order of magnitude for $1/T_{2n}$. From the value of $T_c \approx 0.16$ K, we deduce the electronic dipolar broadening to be $\omega_{\text{int}} \approx 2 \times 10^{10}$ rad/s. With NMR frequencies of order $\omega_n \approx 1.5 \times 10^9$ rad/s the factor $\exp(-\omega_n^2/2\omega_{\text{int}}^2)$ becomes ≈ 1 . Further, we have $B_{\text{tot}} \approx 30$ T and $B_{\text{dip}} \approx (1/3)B_{\text{tot}} \approx 10$ T, yielding $\gamma_n B_{\text{dip}} \approx 6 \times 10^8$ rad/s. For ap-

plied fields $B_a > 5$ T the polarization correction factor $(1 - \tanh^2 X)$ becomes of order 10^{-3} to 10^{-4} . From Eq. (25) with the numerical factors quoted above we thus find the prediction (cf. Fig. 10, dotted line): $1/T_{2n}^{(ED)} \approx 10^4$ to 10^3 s $^{-1}$ for the transverse NSR-rate arising from electron spin-spin interactions, i.e., in the same range as the experimental transverse rate. Conversely, the data clearly show that $1/T_{1n} \ll 1/T_{2n}$, contrary to the prediction of Eq. (25). Indeed, this process basically only establishes the thermal equilibrium between the nuclear and the electronic spin systems, i.e., without considering the relaxation of the latter toward the phonon bath. For the complete description of the nuclear spin-lattice relaxation process we obviously have to investigate the spin-phonon coupling mechanism as well.

In order to estimate the electronic $1/T_{1e}$, we remark that the electron spin-lattice relaxation rate arising from transitions between the two lowest Zeeman levels of the $S=12$ multiplet due to the direct process will be given by the sum of the transition rates w_{\uparrow} and w_{\downarrow} due to absorption and emission of phonons, respectively,⁵²

$$\frac{1}{T_{1e}} = w_{\uparrow} + w_{\downarrow}. \quad (26)$$

Since the phonon modulation of the crystal field can be expected to be the main source of this coupling, we may apply to Mn_6 the calculations developed by Leuenberger and Loss,⁶⁸ obtaining

$$w_{\uparrow} = V_{e-ph}(g\mu_B B_a)^3 \frac{1}{\exp(2X) - 1}, \quad (27a)$$

$$w_{\downarrow} = V_{e-ph}(g\mu_B B_a)^3 \frac{1}{1 - \exp(-2X)}, \quad (27b)$$

$$V_{e-ph} = \frac{D^2 S(2S-1)^2}{6\pi\rho c_s^5 \hbar^4}, \quad (27c)$$

where $S=12$, $D/k_B=0.013$ K is the uniaxial anisotropy constant, $\rho=1.45$ g/cm 3 is the density, and c_s the sound velocity. Within the Debye model, the latter is obtained from the experimental Debye temperature $\Theta_D=29$ K as

$$c_s = \frac{k_B \Theta_D}{\hbar} \left(\frac{6\pi N_A}{V_m} \right)^{-1/3} = 1.3 \times 10^3 \text{ m/s}. \quad (28)$$

Substituting into Eq. (26) yields

$$1/T_{1e} \approx 104 B_a^3 \coth X, \quad (29)$$

with B_a in Tesla. (It should be noted that the value calculated for V_{e-ph} is very sensitive to the values used for Θ_D and D/k_B so that it obviously is subject to a large uncertainty margin.) For instance, $B_a=5$ T and $T=1$ K yields $1/T_{1e} \sim 10^4$ s $^{-1}$. Because of the very small value of the anisotropy constant D in Mn_6 , $1/T_{1e}$ is thus expected to be much lower than the typical values $\sim 10^7$ s $^{-1}$ found, e.g., in Mn_{12} -ac. This also implies that a model for the TSSR rate based on the random changes in local hyperfine field due to electron-phonon excitations, as recently used to describe $1/T_{2n}$ in Mn_{12} -ac,³⁵ would lead in this case to a quantitative estimate that is about

three orders of magnitude lower than our experimental result.

Nuclear relaxation to the lattice can now occur in two ways, either directly via the spin-lattice relaxation fluctuations of the individual electron spins, or in a two-step process by spin-spin relaxation to the electron dipolar reservoir followed by relaxation to the lattice. The direct spin-lattice relaxation (single-ion) process is described by Eq. (24), which becomes

$$\frac{1}{T_{1n}^{(EZ)}} \approx 21 \left(\frac{B_{dip}}{B_{tot}} \right)^2 B_a^3 \coth X (1 - \tanh^2 X). \quad (30)$$

For large X , $\coth X \approx 1$ and $(1 - \tanh^2 X) \approx 4 \exp(-2X)$. With $B_{dip}/B_{tot} \approx 1/3$ one obtains

$$\frac{1}{T_{1n}^{(EZ)}} \approx 9 B_a^3 \exp(-g\mu_B B_a/k_B T), \quad (31)$$

with B_a in Tesla. As we have seen, both the specific heat and the NMR data yield a field dependence of $1/T_{1n}$ that is the same as in Eq. (31), with a prefactor of about 40. The prediction of Eq. (31) is therefore qualitatively satisfactory but quantitatively slightly too low.

Next we consider the two-step relaxation process on basis of the spin-spin interaction process. Intuitively this is easily understood as follows: Relaxation of the nuclei by spin-spin interactions involves $1/T_{2e}$ which will be of order 10^9 Hz or higher, implying that the electron spin-spin interactions can be very effective in relaxing the nuclear spins. However, relaxation is then toward the electron spin system, and the ultimate relaxation to the lattice has to occur in a second step. This situation has often been met for nuclear relaxation in magnetic crystals or in diamagnetic insulators with paramagnetic impurities, notably in connection with the phenomenon of dynamic nuclear polarization.^{65,69,70} In the theoretical treatments it has been proven necessary to consider the Zeeman term and the spin-spin interaction term in the Hamiltonian of a spin system (electronic or nuclear) as separate energy reservoirs, to each of which separate temperatures can be assigned that may differ quite substantially from one another (see Refs. 65 and 70).

Applied to our present problem, this leads to the block diagram sketched in Fig. 11 (the nuclear-dipolar reservoir is omitted here since its energy is so small that it plays no role at the relevant temperatures). The electron-Zeeman (EZ) and electron-dipolar (ED) energy reservoirs will be at the same (lattice) temperature in zero-applied field. However, when with increasing field the electronic level splitting ω_e starts to exceed the electronic dipolar broadening, the two reservoirs become progressively separate entities, characterized by different temperatures and largely different heat capacities. This arises since the EZ reservoir is strongly coupled to the phonon bath and can be considered to remain in equilibrium with the lattice regardless of any nuclear relaxation event. The ED reservoir on the other hand, has a heat capacity that decreases rapidly with field. Although the ED reservoir is coupled to the lattice at a rate $\approx 2/T_{1e}$, i.e., twice the electron spin-lattice relaxation rate,⁷⁰ it is also strongly coupled to the nuclear Zeeman (NZ) system at a rate given by Eq. (25), i.e., of the order of $1/T_{2n}$. In high fields, therefore, the nuclear

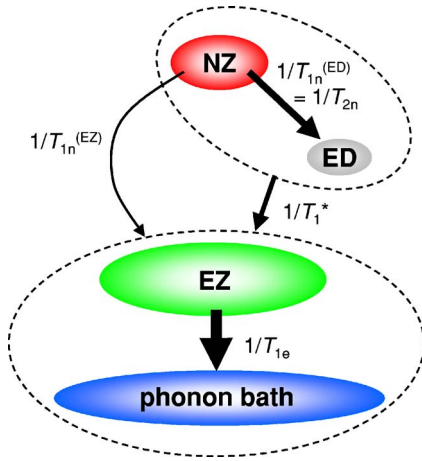


FIG. 11. (Color online) Block diagram of the nuclear and electronic spin systems involved in the relaxation process at high fields, and the relative rates of energy transfer.

relaxation will take place in two stages. In the first stage the NZ and ED systems will become rapidly in equilibrium at basically the same fast rate that determines the experimentally observed $1/T_{2n}$. Subsequently, the coupled NZ+ED systems will relax toward the lattice at the much slower rate,

$$\frac{1}{T_1^*} = \frac{2}{T_{1e}} \frac{C_{ED}}{C_{NZ} + C_{ED}}, \quad (32)$$

which for the case $C_{NZ} \gg C_{ED}$ would become roughly equal to $2/T_{1e}$ (C_{ED}/C_{NZ}). Here the symbols C_{ED} and C_{NZ} stand for the (field-dependent) specific heats of the ED and the NZ reservoirs. The situation is seen to be analogous to the phonon-bottleneck phenomenon, well known in paramagnetic relaxation. Applied to our present case, we calculate C_{NZ} from Eq. (3) to be of order 0.006 R at $T=0.9$ K and $B=5$ T (cf. Figs. 8 and 9), which value depends only weakly on applied field. C_{ED} in zero field can be estimated as⁵²

$$\frac{C_{ED}}{R} = \frac{6}{5} \left(\frac{\mu_0 g^2 \mu_B^2 S(S+1)}{4\pi 3k_B T} \right)^2 \sum_{j>i} \frac{1}{r_{ij}^6}, \quad (33)$$

after averaging over the angular dependence of the dipolar coupling, as appropriate for an unoriented powder sample. Using the same lattice parameters as for the Monte-Carlo simulations yields $C_{ED} \approx 0.004$ R at $T=0.9$ K. C_{ED} then depends on the electronic polarization as $C_{ED}(X) = C_{ED}(0)(1 - \tanh^2 X) \approx 4 C_{ED}(0) \exp(-g\mu_B B_a/k_B T)$, since for high fields only the lowest Zeeman level is available for the electron spins.⁷⁰ All this leads to a global rate for the nuclear spin-lattice relaxation

$$\begin{aligned} \frac{1}{T_1^*} &\approx 208 B_a^3 \coth(X) \frac{0.004(1 - \tanh^2 X)}{0.006 + 0.004(1 - \tanh^2 X)} \\ &\approx 550 B_a^3 \exp(-g\mu_B B/k_B T), \end{aligned} \quad (34)$$

that has the same field dependence as Eq. (31), but with a prefactor of about 550 instead of 9, meaning that the two-step spin-spin relaxation should be the fastest process by almost two orders of magnitude in the high-field region. The

solid line in Fig. 10 is obtained from Eq. (34) but assuming a prefactor of order 25.

At this point it is important to recall that the prefactors in both Eqs. (31) and (34) are affected by a large numerical uncertainty originating from the expression for $1/T_{1e}$, which contains the electron-phonon coupling constant V_{e-ph} , Eq. (27c). This constant is proportional to D^2 and Θ_D^{-5} , and both these quantities have rather large error bars. However, the values of D and Θ_D influence *in the same way* the relaxation rates via the electron-Zeeman and the electron-dipolar channels, thus the latter is expected to dominate *in any case* by almost two orders of magnitude. Due to their strong influence on $1/T_{1e}$, allowing both D and Θ_D to vary by only a factor of 1.5 would already yield the correct quantitative prefactor in Eq. (34).

Summarizing the results of this section, we may state that both the longitudinal and transverse nuclear relaxation that we observe at high applied fields are in excellent qualitative and even quantitative agreement with the model based on fast dipolar relaxation of the hyperfine-coupled nuclear-Zeeman system to the electron-dipolar reservoir, followed by much slower relaxation of the combined systems via the electron spin-lattice channel. The direct nuclear spin-lattice relaxation process by single-ion electron spin-lattice relaxation predicts a similar field dependence but is calculated to be much slower at high fields. At low fields one will have $\omega_e \approx \omega_{int}$, so that the electron-dipolar and the electron-Zeeman systems will become “on speaking terms,” and a subdivision of the two electron spin reservoirs is no longer valid. In this range, however, NSR by means of the scalar hyperfine interaction, Eq. (15), should also become important (since then no longer $\omega_n \ll \omega_e$, whereas $T_{2e} \ll T_{1e}$).

V. CONCLUDING REMARKS

In conclusion, our experiments on Mn_6 show that dipole-dipole interactions between molecular magnetic clusters may indeed induce long-range magnetic order at low temperatures if the anisotropy is sufficiently small. Spin-lattice relaxation is then fast enough to produce equilibrium conditions down to the low temperatures needed. We should add that similar conditions could in principle also be reached in the highly anisotropic cluster systems, for which it was shown that by applying magnetic fields perpendicular to the anisotropy axis, the spin-lattice relaxation can be tuned and made similarly fast through the process of magnetic quantum tunneling. However, it is very rare to observe magnetic ordering phenomena in those systems. One exception known to date²⁸ originates from an unusually high tunneling rate already in zero field. Instead, for the majority of the anisotropic clusters it is likely that, given the magnitude of the fields needed to have a considerable increase of the relaxation rate ($B_{\perp} \gg 1$ T), any longitudinal component of the field would create a Zeeman splitting that is much larger than the energy involved in the magnetic dipolar ordering. We found indeed that in Mn_6 the ordering transition is removed already for relatively small fields (~ 0.5 T). In a recent neutron diffraction experiment on a Mn_{12} -ac single crystal, however, Luis *et al.*⁷¹ achieved an extremely accurate alignment of the field

(to within 0.1 degree) and obtained evidence for a ferromagnetic phase induced by the transverse field.

We have also studied the nuclear spin dynamics of Mn_6 , both directly by NMR experiments and through the hyperfine contribution to the field-dependent specific heat. The agreement between the two techniques is very good, and also provides an interesting comparison with the nuclear spin dynamics in the anisotropic single-molecule magnet Mn_{12} -ac. Both qualitatively and quantitatively, the nuclear magnetic relaxation data turn out to be in good agreement with predictions obtained from theories developed earlier for relaxation in paramagnetic crystals and for dynamic polarization. In high fields, the observed nuclear relaxation is dominated by electron spin fluctuations arising from the dipolar interactions between cluster spins. In spite of the large Zeeman splittings between the cluster-spin levels produced in such high fields, these fluctuations are able to relax the nuclei through the dipolar part of the hyperfine interaction. In this field range the electron dipolar and the electron Zeeman system are basically decoupled. Relaxation of the nuclear spins then proceeds in two steps, namely an initial rapid relaxation to the electron dipolar system via the electron spin-spin interaction channel, followed by a much slower relaxation of the combined nuclear-electron spin systems to the lattice through the electron spin-lattice channel. It is of interest in this regard to note that the values for the longitudinal and transverse relaxation rates as observed for Mn_{12} -ac in the low-temperature ($T < 0.9$ K) quantum regime,³⁶ where the electron spin fluctuations can be attributed to quantum tunnelling of the cluster spins, fall only slightly below the present observations for Mn_6 at $T = 0.9$ K. Below the blocking temperature (~ 3 K) the cluster spins of Mn_{12} -ac become almost fully polarized even in zero field due to the strong crystal-field splittings of the electron spin levels, the distance between the first excited state from the ground state amounting to more than 10 K. The temperature independent value found for the transverse nuclear relaxation rate, $1/T_{2n} \approx 100$ s⁻¹, could be well explained in terms of intercluster nuclear spin diffusion, i.e., nuclear flip-flops arising from the dipolar interaction between nuclear spins in neighboring clusters. The same physical mechanism should also put a lower bound to the transverse nuclear rate in Mn_6 , which is, however, not relevant due to the presence of the faster spin-spin relaxation process.

For the longitudinal rate $1/T_{1n}$ for Mn_{12} -ac a value of ≈ 0.03 s⁻¹ is found below 1 K, slightly depending on temperature. This value agrees with the nuclear-spin-mediated tunneling rate estimated for the fast-relaxing molecular spins in Mn_{12} -ac. As argued by Morello *et al.*,³⁶ the tunneling process can at the same time provide a relaxation channel for the nuclei to the electron-dipolar system. Similar to the above-discussed case of Mn_6 in high field, relaxation to the lattice should then occur in a second step through the electron spin-lattice coupling.

ACKNOWLEDGMENTS

We thank J. Krzystek for performing the high-field EPR study. This work is part of the research program of the

“Stichting voor Fundamenteel Onderzoek der Materie” (FOM) and is partially supported by the European Community Contract No. MRTN-CT-2003-504880 “QUEMOLNA” and by the EC-Network of Excellence “MAGMANet” (Contract No. 515767-2). F.L. acknowledges Grant No. PIP039/2005 from DGA. J.F.F. acknowledges Grant No. BFM2003-03919/FISI, from the MCyT of Spain.

APPENDIX: ESTIMATION OF THE EFFECTIVE DEMAGNETIZING FACTOR

In this Appendix, we derive an approximate expression for the effective demagnetizing factor N_{eff} appropriate for the cylindrically shaped container filled with the grains. This problem is notoriously complex and can only be approximately solved. In a first step the relation should be found between the applied field H_a and the local field H_{loc} acting on a reference grain in the container. Approximating the grains as point dipoles, the difference ($H_{\text{loc}} - H_a$) will be due to the contributions to the field arising from all the other dipoles inside the container. Adopting the well-known Lorentz construction, the dipole summation is split into one inside a (sufficiently large) sphere around the reference grain and a contribution from the dipoles outside this sphere. For this second contribution the dipoles are usually assumed to form a homogeneous continuum so that it is just proportional to the difference in demagnetizing factors of the container (N_{cont}) and of the sphere ($1/3$). As for the first summation, it would be zero for a cubic arrangement of the dipoles. This will not be the case here since the grains are randomly packed, but since a valid estimate is not easily obtained, and we may expect it to be small, we shall just neglect it. One then obtains

$$H_{\text{loc}} = H_a - fM(N_{\text{cont}} - 1/3). \quad (\text{A1})$$

Here f denotes the filling volume fraction of the grains in the container and M is the magnetization of the grains.

In the next step we have to correct H_{loc} for the dipolar contributions arising from the magnetic material inside the grain. In case of a ferromagnetic material, one usually only takes the shape-dependent demagnetizing correction into account. An argument for this may be found in that the magnetization process for the ferromagnet is mostly determined by the mobility of the domain walls, which will react to the macroscopically averaged internal field. For simplicity, we first consider the case of zero magnetocrystalline anisotropy for which the demagnetization factor as well as the magnetization and fields can be treated as scalars. We thus obtain for the internal field H_i inside the grain

$$H_i = H_{\text{loc}} - N_{\text{grain}}M = H_a - N_{\text{grain}}M - fM(N_{\text{cont}} - 1/3). \quad (\text{A2})$$

From the definition: $H_i = H_a - N_{\text{eff}}M$, we thus finally find

$$N_{\text{eff}} = N_{\text{grain}} + f(N_{\text{cont}} - 1/3). \quad (\text{A3})$$

If, by contrast, the grain has uniaxial magnetic anisotropy, we should distinguish between the parallel $\chi_{i,\parallel}$ and the perpendicular $\chi_{i,\perp}$ intrinsic susceptibilities in the response to the

internal magnetic field. These susceptibilities depend on the magnitude of the anisotropy parameter D . They can be obtained, from the numerically calculated eigenstates and eigenvalues of the spin Hamiltonian, using the Van Vleck's formalism as described in, e.g., Ref. 72. In this case Eq. (A2) becomes

$$\mathbf{H}_i = \mathbf{H}_{\text{loc}} - \tilde{N}_{\text{grain}} \tilde{\chi}_i \mathbf{H}_i, \quad (\text{A4})$$

where \tilde{N}_{grain} and $\tilde{\chi}_i$ are respectively the diagonal demagnetizing and intrinsic susceptibility tensors. By combining Eqs. (A1) and (A4) it is possible to find a relationship between the measured susceptibility χ and the two components of $\tilde{\chi}_i$. For

the case when the anisotropy axes are randomly oriented in the sample, we find

$$\chi = \frac{\chi_{\text{eff}}}{1 + f\chi_{\text{eff}}(N_{\text{cont}} - 1/3)}, \quad (\text{A5})$$

where the susceptibility χ_{eff} corrected for the demagnetizing factor of the grains equals

$$\chi_{\text{eff}} = \left[\frac{2\chi_{i,\perp}}{3(1 + \chi_{i,\perp}/3)} + \frac{\chi_{i,\parallel}}{3(1 + \chi_{i,\parallel}/3)} \right]. \quad (\text{A6})$$

This relationship was used to calculate the theoretical powder susceptibilities shown in Fig. 2.

*Corresponding author. Present address: Department of Physics and Astronomy, University of British Columbia, 6224 Agricultural Rd., Vancouver, B.C. V6T 1Z1, Canada. Electronic address: morello@physics.ubc.ca

¹*Quantum Tunneling of the Magnetisation*, edited by L. Gunther and B. Barbara (Kluwer, Dordrecht, 1995).

²E. M. Chudnovsky and J. Tejada, *Macroscopic Quantum Tunneling of the Magnetic Moment* (Cambridge University Press, Cambridge, England, 1998).

³D. Gatteschi and R. Sessoli, in *Magnetism: Molecules to Materials*, edited by J. S. Miller and M. Drillon (Wiley-VCH, Weinheim, 2002), Vol. III, Chap. 3.

⁴I. S. Tupitsyn and B. Barbara, in *Magnetism: Molecules to Materials*, edited by J. S. Miller and M. Drillon (Wiley-VCH, Weinheim, 2002), Vol. III, Chap. 4.

⁵F. Luis, F. L. Mettes, and L. J. de Jongh, in *Magnetism: Molecules to Materials*, edited by J. S. Miller and M. Drillon (Wiley-VCH, Weinheim, 2002), Vol. III, Chap. 5.

⁶R. Sessoli, D. Gatteschi, A. Caneschi, and M. A. Novak, *Nature (London)* **365**, 141 (1993).

⁷D. Gatteschi, A. Caneschi, L. Pardi, and R. Sessoli, *Science* **265**, 1054 (1994).

⁸J. R. Friedman, M. P. Sarachik, J. Tejada, and R. Ziolo, *Phys. Rev. Lett.* **76**, 3830 (1996).

⁹J. M. Hernández, X. X. Zhang, F. Luis, J. Bartolomé, J. Tejada, and R. Ziolo, *Europhys. Lett.* **35**, 301 (1996).

¹⁰L. Thomas, F. Lioni, R. Ballou, D. Gatteschi, R. Sessoli, and B. Barbara, *Nature (London)* **383**, 145 (1996).

¹¹C. Sangregorio, T. Ohm, C. Paulsen, R. Sessoli, and D. Gatteschi, *Phys. Rev. Lett.* **78**, 4645 (1997).

¹²S. M. Aubin, N. R. Dilley, L. Pardi, J. Krzystek, M. W. Wemple, L.-C. Brunel, M. B. Maple, G. Christou, and D. N. Hendrickson, *J. Am. Chem. Soc.* **120**, 4991 (1998).

¹³A. Garg, *Europhys. Lett.* **22**, 205 (1993).

¹⁴W. Wernsdorfer and R. Sessoli, *Science* **284**, 133 (1999).

¹⁵F. L. Mettes, F. Luis, and L. J. de Jongh, *Phys. Rev. B* **64**, 174411 (2001).

¹⁶F. Luis, F. L. Mettes, J. Tejada, D. Gatteschi, and L. J. de Jongh, *Phys. Rev. Lett.* **85**, 4377 (2000).

¹⁷J. F. Fernández and J. J. Alonso, *Phys. Rev. B* **62**, 53 (2000); **65**, 189901(E) (2002).

¹⁸X. Martínez-Hidalgo, E. M. Chudnovsky, and A. Aharony, *Euro-*

phys. Lett. **55**, 273 (2001).

¹⁹S. J. White, M. R. Roser, J. Xu, J. T. van der Noordaa, and L. R. Corruccini, *Phys. Rev. Lett.* **71**, 3553 (1993).

²⁰M. R. Roser and L. R. Corruccini, *Phys. Rev. Lett.* **65**, 1064 (1990).

²¹Although one might have thought the ordering of nuclear moments to present an example, this certainly does not hold for the simple metals (Cu, Ag), for which it turns out that exchange interactions of the RKKY type play an important if not overwhelming role. A similar remark holds for many rare-earth compounds.

²²T. Lis, *Acta Crystallogr., Sect. B: Struct. Crystallogr. Cryst. Chem.* **B36**, 2042 (1980).

²³K. Wieghardt, K. Pohl, I. Jibril, and G. Huttner, *Angew. Chem., Int. Ed. Engl.* **23**, 77 (1984).

²⁴S. M. Aubin, M. W. Wemple, D. M. Adams, H.-L. Tsai, G. Christou, and D. N. Hendrickson, *J. Am. Chem. Soc.* **118**, 7746 (1996).

²⁵N. Aliaga, K. Folting, D. N. Hendrickson, and G. Christou, *Polyhedron* **20**, 1273 (2001).

²⁶F. L. Mettes, G. Aromí, F. Luis, M. Evangelisti, G. Christou, D. Hendrickson, and L. J. de Jongh, *Polyhedron* **20**, 1459 (2001).

²⁷J. F. Fernández, *Phys. Rev. B* **66**, 064423 (2002).

²⁸M. Evangelisti, F. Luis, F. L. Mettes, N. Aliaga, G. Aromí, J. J. Alonso, G. Christou, and L. J. de Jongh, *Phys. Rev. Lett.* **93**, 117202 (2004).

²⁹A. Morello, F. L. Mettes, F. Luis, J. F. Fernández, J. Krzystek, G. Aromí, G. Christou, and L. J. de Jongh, *Phys. Rev. Lett.* **90**, 017206 (2003).

³⁰G. Aromí, M. J. Knapp, J.-P. Claude, J. C. Huffman, D. N. Hendrickson, and G. Christou, *J. Am. Chem. Soc.* **121**, 5489 (1999).

³¹M. Affronte, J. C. Lasjaunias, W. Wernsdorfer, R. Sessoli, D. Gatteschi, S. L. Heath, A. Fort, and A. Rettori, *Phys. Rev. B* **66**, 064408 (2002).

³²A. Yamaguchi, N. Kusumi, H. Ishimoto, H. Mitamura, T. Goto, N. Mori, M. Nakano, K. Awaga, J. Yoo, D. N. Hendrickson, and G. Christou, *J. Phys. Soc. Jpn.* **71**, 414 (2002).

³³A. Bino, D. C. Johnston, D. P. Goshorn, T. R. Halbert, and E. I. Stiefel, *Science* **241**, 1479 (1988).

³⁴Y. Furukawa, K. Watanabe, K. Kumagai, F. Borsa, and D. Gatteschi, *Phys. Rev. B* **64**, 104401 (2001).

³⁵T. Goto, T. Koshihara, T. Kubo, and K. Agawa, *Phys. Rev. B* **67**,

- 104408 (2003).
- ³⁶A. Morello, O. N. Bakharev, H. B. Brom, R. Sessoli, and L. J. de Jongh, *Phys. Rev. Lett.* **93**, 197202 (2004).
- ³⁷A. Morello, Ph.D. thesis, Leiden University, March 2004, cond-mat/0404049.
- ³⁸F. L. Mettes, Ph.D. thesis, Leiden University, September 2001.
- ³⁹A. Bencini and D. Gatteschi, *EPR of Exchange Coupled Systems* (Springer-Verlag, Berlin, 1990).
- ⁴⁰See, e.g., J. J. M. Steijger, E. Frikkee, L. J. de Jongh, and W. J. Huiskamp, *Physica B & C* **123**, 271 (1984).
- ⁴¹J. A. Mydosh, *Spin Glasses: An Experimental Introduction* (Taylor and Francis, London, 1993).
- ⁴²D. H. Reich, B. Ellman, J. Yang, T. F. Rosenbaum, G. Aeppli, and D. P. Belanger, *Phys. Rev. B* **42**, 4631 (1990).
- ⁴³D. H. Reich, T. F. Rosenbaum, and G. Aeppli, *Appl. Phys. Lett.* **59**, 1969 (1987).
- ⁴⁴S. Ghosh, R. Parthasarathy, T. F. Rosenbaum, and G. Aeppli, *Science* **296**, 2195 (2002).
- ⁴⁵M. R. Roser, J. Xu, S. J. White, and L. R. Corruccini, *Phys. Rev. B* **45**, 12337 (1992).
- ⁴⁶A. H. Cooke, D. A. Jones, J. F. A. Silva, and M. R. Wells, *J. Phys. C* **8**, 4083 (1975).
- ⁴⁷P. Beauvillain, J.-P. Renard, I. Laursen, and P. J. Walker, *Phys. Rev. B* **18**, 3360 (1978).
- ⁴⁸J. Als-Nielsen, *Phys. Rev. Lett.* **37**, 1161 (1976).
- ⁴⁹D. H. Reich, T. F. Rosenbaum, G. Aeppli, and H. J. Guggenheim, *Phys. Rev. B* **34**, 4956 (1986).
- ⁵⁰T. Moriya, in *Magnetism*, edited by G. T. Rado and H. Suhl, Vol. I (Academic Press, New York, 1963), Chap. 3.
- ⁵¹L. J. de Jongh and A. R. Miedema, *Adv. Phys.* **50**, 947 (2001).
- ⁵²A. Abragam and B. Bleaney, *Electron Paramagnetic Resonance of Transition Ions* (Oxford University Press, London, 1970).
- ⁵³A. Abragam, *The Principles of Nuclear Magnetism* (Oxford University Press, London, 1961).
- ⁵⁴A. Suter, M. Mali, J. Roos, and D. Brinkmann, *J. Phys.: Condens. Matter* **10**, 5977 (1998).
- ⁵⁵T. Kubo, T. Goto, T. Koshiba, K. Takeda, and K. Awaga, *Phys. Rev. B* **65**, 224425 (2002). See also T. Kubo, A. Hirai, and H. Abe, *J. Phys. Soc. Jpn.* **26**, 1094 (1969).
- ⁵⁶A. Lascialfari, Z. H. Jang, F. Borsa, P. Carretta, and D. Gatteschi, *Phys. Rev. Lett.* **81**, 3773 (1998).
- ⁵⁷Z. Salman, cond-mat/0209497 (unpublished).
- ⁵⁸B. Pilawa, R. Boffinger, I. Keilhauer, R. Leppin, I. Odenwald, W. Wendl, C. Berthier, and M. Horvatić, *Phys. Rev. B* **71**, 184419 (2005).
- ⁵⁹C. P. Slichter, *Principles of Magnetic Resonance* (Springer-Verlag, Berlin, 1978).
- ⁶⁰T. Moriya, *Prog. Theor. Phys.* **16**, 23 (1956).
- ⁶¹T. Moriya and Y. Obata, *J. Phys. Soc. Jpn.* **13**, 1333 (1958).
- ⁶²T. Moriya, *J. Phys. Soc. Jpn.* **13**, 1344 (1958).
- ⁶³R. Kubo and K. Tomita, *J. Phys. Soc. Jpn.* **9**, 888 (1954).
- ⁶⁴N. Bloembergen, *Physica (Amsterdam)* **15**, 386 (1949).
- ⁶⁵A. Abragam and M. Goldman, *Nuclear Magnetism: Order and Disorder* (Clarendon Press, Oxford, 1982).
- ⁶⁶T. E. Gunter and C. D. Jeffries, *Phys. Rev.* **159**, 290 (1967).
- ⁶⁷I. J. Lowe and D. Tse, *Phys. Rev.* **166**, 279 (1968).
- ⁶⁸M. N. Leuenberger and D. Loss, *Phys. Rev. B* **61**, 1286 (2000).
- ⁶⁹A. Abragam and M. Borghini, *Prog. Low Temp. Phys.* **4**, 384 (1964).
- ⁷⁰G. R. Khutsishvili, *Prog. Low Temp. Phys.* **6**, 375 (1970).
- ⁷¹F. Luis, J. Campo, J. Gómez, G. J. McIntyre, J. Luzón, and D. Ruiz-Molina, *Phys. Rev. Lett.* **95**, 227202 (2005).
- ⁷²R. L. Carlin, *Magnetochemistry* (Springer-Verlag, Berlin, 1986), Chap. II.